NASA
Technical
Paper
2504

December 1985

Development of a UHF Radiometer

Bruce M. Kendall,
Hans-Juergen C. Blume,
and Aubrey E. Cross

NASA

NASA Technical Paper 2504

1985

Development of a UHF Radiometer

Bruce M. Kendall,
Hans-Juergen C. Blume,
and Aubrey E. Cross

Langley Research Center
Hampton, Virginia

National Aeronautics
and Space Administration

Scientific and Technical Information Branch

SUMMARY

A wideband multifrequency UHF radiometer was initially developed to operate in the 500- to 710-MHz frequency range for the remote measurement of ocean water salinity. However, radio-frequency interference required a reconfiguration to operate in the single-frequency radio astronomy band of 608 to 614 MHz. Details of the radiometer development and testing are described. Flight testing over variable terrain provided a performance comparison of the UHF radiometer with an L-band radiometer for remote sensing of geophysical parameters. Although theoretically more sensitive, the UHF radiometer was found to be less desirable in practice than the L-band radiometer.

INTRODUCTION

The results of several aircraft programs have demonstrated that geophysical parameters such as temperature, salinity, and thickness of oil spills can be derived from passive microwave measurements with an accuracy that satisfies most user applications (ref. 1). In particular, a technique to remotely measure sea-surface temperature and salinity was demonstrated with a dual-frequency microwave radiometer system (ref. 2). Accuracies in temperature of $1^{o}C$ and in salinity of 1 part per thousand ($^{o}/oo$) for salinity greater than 5 $^{o}/oo$ were attained after correcting for the influence of extraterrestrial background radiation, atmospheric radiation and attenuation, sea-surface roughness, and antenna beamwidth. The radiometers, operating at 1.43 and 2.65 GHz, comprise a third-generation system using null balancing and feedback noise injection. This dual-frequency microwave radiometer system was developed at the NASA Langley Research Center for the purpose of obtaining sea-surface temperature and salinity maps of coastal and estuarine areas.

However, the requirements for the measurement of open-ocean salinity are different and much more stringent. In order to infer measurements of seawater mass density from the simultaneous measurement of temperature and salinity, the accuracy requirements cited by some oceanographers would require the measurement of salinity with an accuracy of 10 parts per million (ref. 3). Previous studies (ref. 4) had shown that an increased sensitivity in the change in radiometer brightness temperature for a corresponding change in salinity occurred with decreasing microwave frequencies. Therefore, a development program was initiated at the NASA Langley Research Center for a UHF radiometer to operate within a frequency band of 500 to 710 MHz, which by virtue of its lower frequency (below the previous 1.43-GHz radiometer), should have been able to measure salinity with an accuracy of a fraction of 1 $^{o}/oo$. This developmental effort, including instrument design, testing, associated problem areas, results, and conclusions, is described in this report.

ACKNOWLEDGMENTS

The authors wish to acknowledge the support and assistance of M. C. Bailey for the phased-array antenna development, E. S. Bradshaw, and H. F. Thornton for the RF component testing, C. P. Hearn for the antenna VSWR flight measurement system design, and J. J. Davis for the RFI flight measurements. All were members of the staff of the NASA Langley Research Center. Also, acknowledgment is given to C. A. Lipp, Jr.,

of PRC Kentron, Inc., for the testing, installation, and calibration of the system and to C. A. Breiner of the same firm for the system mechanical design. We wish to express our thanks to Clayton B. Jackson of the Research Triangle Institute and Nancy D. Turner of Bionetics Corp. for assistance in the data reduction. Finally, we want to thank the NASA Wallops Flight Facility staff, especially P. Bradfield, for their valuable assistance and aircraft support.

SYMBOLS

B	predetection bandwidth, Hz
e	emissivity at nadir of calm sea surface, dimensionless
$e(\theta,T_s)$	emissivity of sea at molecular temperature T_s for viewing angle θ, dimensionless
e_λ	emissivity at wavelength λ, dimensionless
f	frequency, GHz
h	aircraft altitude, km
S	salinity, parts per thousand ($^o/oo$)
$\langle T \rangle$	average physical temperature of intervening atmosphere, K
T_{atm}	terrestrial sky brightness temperature at viewing angle θ, K
T_B	sea-surface brightness temperature, K
T_c	total extraterrestrial background radiation temperature, K
T_{cos}	thermal component of cosmic background radiation, K
T_{gal}	galactic noise temperature, K
$T_o(h)$	equivalent atmospheric noise temperature at altitude h, K
T_R	radiometer apparent temperature, K
T_{rec}	receiver input noise temperature, K
T_{ref}	reference load temperature, K
T_s	sea-surface molecular temperature, K or ^oC
T_{sky}	sky background temperature, K
$T(z)$	atmospheric physical temperature at altitude z, K
$T(z,\theta)$	atmospheric physical temperature at altitude z and viewing angle θ, K
z	altitude, km

$\alpha(z)$ atmospheric absorption coefficient at altitude z, dimensionless

$\alpha(z,\theta)$ atmospheric absorption coefficient at altitude z and viewing angle θ, dimensionless

Γ voltage reflection coefficient

ΔT radiometer sensitivity, K

ΔT_p antenna pattern temperature correction, K

θ viewing angle from nadir, rad

λ wavelength, cm

σT_A^1 error in brightness temperature calculated from sky measurement antenna loss and calibration factor, K

σT_A^2 error in brightness temperature calculated from calibration factor inverted from sea-truth data, K

τ integration time, sec

$\tau(h)$ atmospheric opacity at altitude h, dimensionless

τ_o total one-way atmospheric opacity, dimensionless

$\tau(z)$ atmospheric opacity at altitude z, dimensionless

Abbreviations and Acronyms:

BP band-pass

BW bandwidth

CF center frequency

DVM digital voltmeter

HP high-pass

IF intermediate frequency

LNA low-noise amplifier

LN_2 liquid nitrogen

LP low-pass

PBMR pushbroom microwave radiometer

RF radio-frequency

RFI radio-frequency interference

R/V research vessel

SFMR stepped frequency microwave radiometer

UHF ultrahigh frequency

VSWR voltage standing wave ratio

MICROWAVE BRIGHTNESS TEMPERATURE MODEL

Radiative Transfer Equation

Quantitative measurements of the thermal emission from the sea surface require corrections for the radiative and transmission properties of the intervening atmosphere and sky, antenna beam efficiency, and sea-surface roughness. In addition to the thermal emission from the sea surface, a microwave radiometer will receive additional contributions of the upwelling radiation from the atmosphere and reflected radiation downwelling from the atmosphere, the cosmic background, the galaxy, and the Sun (ref. 2). If a specular ocean surface is assumed, the apparent temperature T_R (which may also be called the equivalent radiometric temperature of the complete set of received radiations) can be calculated from the equation of radiative transfer by making use of the Rayleigh-Jeans approximation to the Planck law (ref. 2) as follows:

$$T_R(\theta) = \left[1 - e(\theta,T_s)\right]\left\{T_c \exp\left[-\int_0^\infty \alpha(z,\theta)\,dz\right] + \int_0^\infty T(z,\theta) \exp\left[-\int_0^z \alpha(z,\theta)\,dz\right]\alpha(z,\theta)\,dz\right\}\exp\left[-\int_0^h \alpha(z,\theta)\,dz\right] + e(\theta,T_s)\,T_s \exp\left[-\int_0^h \alpha(z,\theta)\,dz\right] + \int_0^h T(z,\theta) \exp\left[-\int_0^z \alpha(z,\theta)\,dz\right]\alpha(z,\theta)\,dz \qquad (1)$$

where

$e(\theta,T_s)$ emissivity of sea at molecular temperature T_s for nadir-viewing angle θ

h altitude of aircraft

T_c total extraterrestrial background radiation temperature

$T(z,\theta)$ temperature of atmosphere at altitude z and viewing angle θ

$\alpha(z,\theta)$ atmospheric absorption coefficient at z and θ

The first term in equation (1) comprises the temperature of the downward radiation of the extraterrestrial noise, attenuated by the entire atmosphere, and the downward radiation of the atmosphere itself, reflected by the ocean surface and in turn attenuated by the intervening atmosphere between the ocean and the radiometer. The second term accounts for the attenuated emission from the ocean surface. The third term accounts for the upward emission of the atmosphere between the ocean and the radiometer.

Since the antenna gain pattern for most radiometers is highly directional and falls off rapidly with increasing θ, a horizontally stratified atmosphere model can be used to approximate equation (1) by replacing the nested integrals with opacities $\left(\text{i.e., } \tau(z) = \int_0^z \alpha(z)\, dz\right)$ as follows:

$$T_R(\theta) = [1 - e(\theta,T_s)]\left\{T_c \exp(-\tau_o \sec\theta) + \int_0^\infty T(z) \exp[-\tau(z) \sec\theta]\, \alpha(z) \sec\theta\, dz\right\} \exp[-\tau(h) \sec\theta] + e(\theta,T_s)\, T_s \exp[-\tau(h) \sec\theta] + \int_0^h T(z) \exp[-\tau(z) \sec\theta]\, \alpha(z) \sec\theta\, dz \qquad (2)$$

where τ_o is the total one-way opacity of the atmosphere, and $\tau(h)$ and $\tau(z)$ are the opacities at altitudes h and z, respectively.

At frequencies below 1 GHz, the opacity is small, and a linear approximation of the exponential terms in equation (2) can be made. Therefore, all $\{\exp[-\tau(z) \sec\theta]\}$ terms can be approximated by the term $[1 - \tau(z) \sec\theta]$. Also, for a nadir-viewing antenna, $\theta = 0$ and the $[1 - \tau(z) \sec\theta]$ term becomes $[1 - \tau(z)]$.

The extraterrestrial background radiation (T_c) consists of galactic noise (T_{gal}), the thermal component of cosmic background radiation (T_{cos}), and emission from strong radio sources such as the Sun. Since the Sun is a point source, its contribution depends strongly on the antenna viewing angle, the Sun's position, the antenna pattern, and the roughness of the sea surface. The noise radiation temperature of the Sun increases greatly at frequencies below 1 GHz, and at 600 MHz it is on the order of 500 000 K. This emission is so great that solar radiation reflected into the radiometer antenna beam could cause measurement error and even saturate the radiometer itself. Therefore, it is important that operation of a radiometer at a frequency less than 1 GHz be restricted to a time of day when reflected solar radiation would be at a minimum or to nighttime only. If this condition can be met, then

$$T_c = T_{gal} + T_{cos} \qquad (3)$$

The magnitude of T_{gal} is dependent upon direction, because of the nonuniformity of radiation emitted by the various sections of the galaxy (ref. 5), and frequency. The

galactic noise temperature (T_{gal}) is a maximum in the direction of the galaxy center and a minimum at the galactic pole. The frequency dependence of T_{gal} seems to vary between $f^{-2.5}$ and f^{-3}, depending on the particular galactic sector. Apinis and Peake (ref. 6) have proposed a model which uses an $f^{-2.7}$ dependence. This model indicates a possible range for T_{gal} of 8 to 151 K at a frequency of 611 MHz, depending on which part of the galaxy is being viewed. This wide range of T_{gal} values poses a problem for the use of microwave radiometers for observations of surfaces which are highly reflective at microwave frequencies, such as ocean waters, and presents a serious problem for the accurate measurement of salinity. One technique to remove the associated bias of a variable galactic background contribution is to use a separate antenna to simultaneously measure the sky background during Earth observation measurements. Another is to map the sky background with the same Earth-viewing radiometer over continuous 24-hour periods and in the same geographic locations as the Earth observation measurements to obtain a model. Both techniques were investigated and are described in this paper.

The symbol T_{cos} represents the cosmic microwave radiation and is frequency independent over the microwave frequency band. Values of T_{cos} of about 2.7 K were reported earlier (ref. 7), but more recent published data (ref. 8) indicated its value now to be around 3 K. For the clear atmosphere, water vapor and molecular oxygen are the main sources of microwave attenuation. However, for frequencies below 1 GHz, the contribution due to water vapor is negligible. Therefore, the atmospheric absorption and hence radiation are dominated by molecular oxygen.

The brightness temperature T_{atm} of the terrestrial sky at zenith angle θ is

$$T_{atm} = \int_0^\infty T(z) \exp[-\tau(z) \sec \theta] \alpha(z) \sec \theta \, dz \tag{4}$$

which contains the atmospheric term of equation (2). Previous measurements (ref. 2) for the clear atmosphere at 2.65 GHz indicated that the zenith brightness temperature and, therefore, the opacity of the cloudless terrestrial sky, are consistent with the predictions of the Van Vleck-Weisskopf model for oxygen absorption. For 611 MHz, the theory predicts values of 1.6 K and 0.006 for T_{atm} and τ_o, respectively.

The last term of equation (2), which is the equivalent noise temperature of the intervening atmosphere, can be rewritten (with $\sec \theta = 1$) as

$$T_o(h) = \int_0^h T(z) \exp[-\tau(z)] \alpha(z) \, dz \tag{5}$$

The atmospheric opacity, or attenuation, $\tau(h)$ and equivalent noise temperature $T_o(h)$ of the 1962 U.S. Standard Atmosphere have been previously evaluated at 1.43 and 2.65 GHz (ref. 2). It was shown that for altitudes less than 2 km, which are representative of remote sensing from an aircraft platform, the opacity $\tau(h)$ is approximately linear with altitude. A similar analysis to that reported in reference 2 was used to obtain a value for $\tau(h)$ equal to 0.001087h for the UHF band, where h is the height in kilometers. Therefore, the right side of equation (5) (for $h < 2$ km) can be approximated by $\langle T \rangle \tau(h)$ where $\langle T \rangle$ is

the average physical temperature of the intervening atmosphere between the radiometer and the sea surface. A similar analysis to that in reference 2 yielded a value of 284.9 K for $\langle T \rangle$ for the UHF band.

By applying the preceding approximations and derivations and replacing the term $e(\theta,T_s)$ with e (the nadir emissivity of a calm sea surface) and the term $e(\theta,T_s)T_s$ with the sea-surface brightness temperature T_B, equation (2) simplifies to

$$T_R = T_B[1 - \tau(h)] + (1 - e)[1 - \tau(h)]\left[(T_{cos} + T_{gal})(1 - \tau_o) + T_{atm}\right] + \tau(h)\langle T \rangle + \Delta T_p \quad (6)$$

where the last term ΔT_p is added to account for the antenna pattern deviations from the ideal "pencil" beam shape (ref. 2). At some microwave frequencies, an additional term for surface roughness correction is necessary because of a dependency of emissivity on roughness. However, it has been demonstrated that these effects diminish with decreasing frequency and are negligible at L-band and below (ref. 9).

Sea-Surface Brightness Temperature

The brightness temperature measured by an ideal radiometer is related to the molecular temperature of a radiating surface via the emissivity of the surface. The emissivity of a dielectric surface at a particular wavelength is determined by its complex dielectric constant, which for seawater is a function only of temperature and salinity. Therefore, the brightness temperature of the sea surface is given by

$$T_B(\lambda) = e_\lambda(T_s,S)\, T_s \quad (7)$$

where emissivity e at the wavelength λ is expressed in terms of surface temperature T_s and salinity S. A plot of brightness temperature as a function of salinity and surface temperature at 620 MHz is given in figure 1. This curve was derived in a similar manner to those reported in reference 2 for 1.43 and 2.65 GHz. Thus, if an independent measurement of sea-surface temperature is obtained, as one from an infrared radiometer, then a UHF radiometer brightness temperature measurement can be inverted to obtain a measurement of sea-surface salinity. The dual inversion of microwave brightness temperatures from two radiometers by using derived regression equations to provide values of both sea-surface temperature and salinity is well documented in the open literature (refs. 1 and 2).

However, there are errors associated with this inversion process. A study was performed to determine the sensitivity of the errors associated with the determination of surface temperature and salinity as a function of the errors associated in the measured brightness temperatures with combinations of UHF, S- and C-band, and infrared radiometers. The results of this study are reported in reference 10. For a typical measurement of the sea surface at 20°C and 30 °/oo, this study indicates that using a UHF and an infrared radiometer pair with a UHF sensitivity of 0.3 K would result in an error of 0.95 °/oo in the measurement of sea-surface salinity. This is not a significant improvement over the obtained accuracy of 1 °/oo as reported in reference 2 for an L- and S-band radiometer pair. Therefore, the possibility exists that the required measurement accuracy of fractions of 1 °/oo for open-ocean salinity

may not be obtainable even with a UHF radiometer. This issue is addressed in the following discussions.

WIDEBAND MULTIFREQUENCY RADIOMETER DEVELOPMENT

The UHF radiometer (500 to 710 MHz) design is like that of the previously developed L- and S-band systems (ref. 2), that is, a Dicke-type radiometer with noise injection and null-balancing features. The antenna is a nadir-looking linearly polarized phased array enclosed in a thermally controlled radome, like that of the L-band system. In addition, a zenith-looking single-element antenna in a radome was initially developed to measure background radiation corrections for the UHF-measured brightness temperature of the sea surface.

Receiver

A block diagram of the receiver design is shown in figure 2. The input directional coupler adds 40-μsec-wide noise pulses to the received radiation. The Dicke switch, in this case a diode switch with a built-in matched load on one port, switches between the incoming radiation (with added injected noise) and the reference load, which is kept at a constant temperature of 308.2 ± 0.03 K. The band-pass filter is a low-loss and low-VSWR (voltage standing wave ratio) rejection filter with respect to radio-frequency interference (RFI). The isolator is a compensation device which prevents input noise changes of the following amplifier from being reflected back into the antenna input point. The low-noise preamplifier (1 dB noise figure) is specially designed for wide-bandwidth (210-MHz) operation, constant amplificaton (30 dB) over the bandwidth, and linear amplification to prevent cross modulation of RFI into the operating frequency band. The two seven-position latching switches allow selection of the seven band-pass filters for the desired channel. Six filters with 60-MHz bandwidths cover the 210-MHz band with center frequencies of 530, 560, 590, 620, 650, and 680 MHz. The seventh filter with a center frequency of 605 MHz and a bandwidth of 210 MHz is for maximum radiometer sensitivity because of its wide bandwidth. The second amplifier increases the signal to the maximum level compatible with linear mixer operation. The local oscillator is voltage controlled to permit center frequency changes corresponding to the center frequency of the selected band-pass filter. By using preset voltage levels in the control electronics circuitry, simultaneous selection of the desired filter and corresponding local oscillator center frequency are accomplished by means of push-button controls.

The IF amplifier with the high-pass filter, the second bank of 5- and 30-MHz low-pass filters, and a no-filtering connection make the receiver more selective in preventing RFI. The second bank of filters is controlled by three-position latching switches, which are in turn controlled by push buttons on the electronics control panel. The square-law detector allows the radiometer output to be directly linear with brightness temperature. The synchronous detector in cooperation with the Dicke generator compares the two detected signals (received radiation plus injected noise and the reference load noise) and drives the voltage-to-frequency converter to change the injected noise pulse frequency when the received radiation changes. This brings the feedback to a new noise power level to balance the output of the receiver.

The multichannel (center frequency) feature of the receiver design allows the manual selection of a particular channel free of RFI from UHF TV stations and/or UHF communication units. The physical layout of the above-described receiver components is shown in figure 3. The receiver unit is maintained at a uniform temperature

of 308.2 K to insure that all the front-end losses remain constant. The constant temperature is accomplished by temperature control of a thermally insulated receiver enclosure, which is shown in figure 4 with all the interconnecting components.

Performance testing of the receiver was accomplished by use of a matched termination at the input which was emersed in liquid nitrogen to provide a constant brightness temperature of 77.4 K. The results of the tests are shown in table I,

TABLE I.- RECEIVER SENSITIVITY TEST RESULTS

Center frequency, MHz	Bandwidth, MHz	ΔT, K (τ = 1 sec)	
		Theory	Measured
530	60	0.1	0.18
	10	.24	.27
560	60	.1	.15
	10	.24	.32
590	60	.1	.15
	10	.24	.32
620	60	.1	.2
	10	.24	.25
650	60	.1	.18
	10	.24	.25
680	60	.1	.15
	10	.24	.2
605	120	.053	.1

where the sensitivity (ΔT), both theoretical and measured, is shown for each center frequency and bandwidth. The theoretical sensitivity was calculated by

$$\Delta T = \frac{2(T_{ref} + T_{rec})}{\sqrt{B_\tau}} \tag{8}$$

where

T_{ref} reference load temperature, K

T_{rec} receiver input noise temperature, K

B predetection bandwidth, Hz

τ integration time, sec

It should be noted that the bandwidths listed in table I are twice those of the corresponding low-pass filter bandwidths as shown in figure 2. The reason is that the local oscillator is tuned to the center frequency of the band-pass filters, and a fold-over of the sidebands takes place in the balanced mixer.

To maintain continuity of calibration between the different channels, the noise source output level was controlled with a channel-dependent bias, so that each channel produced the same output for an input of 77.4 K. The resulting agreement was 77.63 ± 0.51 K.

Antenna

The antenna system for the UHF radiometer consisted of a linearly polarized array of 36 bow-tie elements in a thermal enclosure (ref. 11). The bow-tie element configuration, shown in figure 5, was chosen for its wide bandwidth characteristic. The 6 × 6 array of this configuration utilized baffles between adjacent rows, as seen in figure 6, to reduce coupling. The 36 elements were connected in groups of 3 to 12 power-combining circuit boards, which in turn were connected to 4 power-combining boards whose outputs were finally combined by a single power-combining circuit to produce the antenna output to the radiometer. The physical stacking of these boards is shown in figure 7, and a partial assembly of the first-layer array of the stacking is shown in figure 8. The complete antenna assembly, housed in its thermal enclosure, is shown in figure 9. This array was designed to operate over the frequency band of 500 to 700 MHz. Representative antenna patterns at 620 MHz are shown in figures 10(a) and (b) for vertical and horizontal polarization, respectively. It can be seen that the 3-dB beamwidth is about 20°. The return loss (reflection coefficient) of the antenna array, as seen by the radiometer, was measured over the 500- to 700-MHz band and is shown in figure 11.

The sky antenna, shown in figure 12, consisted of a single bow-tie element in a radome mounted on the top of the aircraft. It was connected to the radiometer receiver via a low-loss coaxial cable.

Radiometer Assembly

The complete radiometer system assembly, consisting of the receiver, junction box, and antenna is shown in figures 13(a) and (b). These figures show a metal framework supporting the fiberglass thermal enclosure of the phased-array antenna and the receiver thermal enclosure. The junction box connects the receiver electronics to the control electronics housed in a relay rack. The supporting framework was designed to mount the UHF radiometer system in the bomb-bay area of a P-3 aircraft. Figure 14 shows the assembled radiometer system suspended over a liquid nitrogen (LN_2) cold load, used for calibration, and the relay rack containing the control and data processing electronics.

Cold-Load Tests

Using the cryogenic RF cold-load setup shown in figure 14, the radiometer was calibrated (ref. 2), the antenna loss measured, and the system ΔT determined. Since the radiometer receiver with the antenna attached is an open system, it was susceptible to radio-frequency interference (RFI), mainly from UHF television stations. Because of this, only the frequency bands of 650 and 680 MHz were able to be used for the cold-load testing at Langley. The cold-load calibration of the radiometer, as described in reference 2, is a well-established technique. The antenna loss was measured by varying the physical temperature of the antenna by means of the antenna temperature control system and measuring the corresponding change in radiometric brightness temperature. The measured mean antenna loss at 680 MHz was 1.14 dB. This value compares favorably with the sum of the individual path losses of the antenna power divider circuit, which was measured independently as 1.09 dB.

The sky antenna was also calibrated in a similar manner with the radome suspended over the same cold load and shrouded with an aluminized polyester film cover. The antenna loss for this single-element antenna was actually the loss of the low-loss RF cable used to connect it to the radiometer receiver. This measured value was 0.4 dB at 680 MHz.

The measured sensitivity of the radiometer system at 680 MHz with a 60-MHz bandwidth and a 1-sec integration time was 0.2 K. The sensitivity calculated from the system losses and reflection coefficients was 0.16 K, which compares favorably with the measured values. These values are slightly higher than those shown in table I, as they include the effects of the antenna.

The absolute accuracy of this calibration method can be adversely affected when both the cold load and the antenna have nonnegligible reflection coefficients, since a situation will exist which permits multiple-reflection effects. In calibrating the UHF radiometer, multiple-reflection effects were observed to be larger than those which had been encountered with higher frequency radiometers at L-, S-, and C-bands. Adjustment of the separation between the antenna and the cold-load surface produced variations in the indicated brightness temperature of as much as several kelvins. Because of this and RFI effects, subsequent cold-load calibrations of the receiver only were based on the use of a precision coaxial cold load ($|\Gamma| \approx 0$). The radiometric uncertainty associated with a nonideal cold-load—horn calibration is the subject of an ongoing investigation.

Several tests were conducted on the receiver itself with precision coaxial terminations immerged in LN_2 and connected to both the nadir and sky antenna ports. In addition to the receiver sensitivity being measured as previously discussed (see table I), a series of tests were performed on the repeatability of the antenna switch by continuously switching between the nadir and sky antenna ports while they were connected to the matched loads immerged in LN_2. These tests were conducted over several successive days and then repeated over several weeks. The results indicated no deviation in output any greater than 0.1 K, which was within the accuracy of the measurement.

Flight Tests

Several flight tests were flown onboard the NASA P-3 aircraft from the NASA Wallops Flight Facility, Wallops Island, Virginia, during the summer of 1982 and prior to the functional test flight to measure sea-surface salinity. The first

series of flight tests were conducted to measure the frequency of possible radio-frequency interference (RFI) signals. Although the radiometer was designed with multiple frequency channels and bandwidth capability to avoid RFI, a prior knowledge of possible RFI would be useful. Therefore, a single UHF bow-tie antenna element enclosed in a radome mounted on the bottom of the P-3 aircraft (nadir viewing) and a spectrum analyzer were used to measure RFI on June 23 and 24 and August 17, 1982, over the Atlantic Ocean east and southeast of Wallops Island at distances up to 175 n.mi. (324 km). These tests were flown over the areas intended for the functional radiometer flight testing at an altitude of 500 ft (152 m). Examples of obtained data are shown in figure 15(a) (175 n.mi. from Wallops) and figure 15(b) (near Wallops). These results showed appreciable RFI levels even at a distance from land (RFI source) of 175 n.mi. It became obvious from these results that an RFI signal could possibly be present in all the radiometer channels if the wide bandwidth (60 MHz) was used. Therefore, it was decided to use only the narrow bandwidth (at a reduced sensitivity) for the functional test flight.

The second type of flight test was concerned with measuring the change in the radiometer phased-array antenna return loss during conditions of flight vibration. This test was deemed important, as the antenna has a large and variable return loss over the operating bandwidth, as seen in figure 11. Even small variations in the return loss during a flight measurement would cause appreciable changes and/or errors in the measured brightness temperature. This particular antenna, because of the long associated wavelengths for the UHF band, had printed-circuit-type power-divider boards which were long and flexible. Thus, if not sufficiently supported and/or strong enough, they might experience vibration flexing during flight with a resulting change in antenna return loss. A flight test made on August 13, 1982, indicated an apparent return loss change ranging from 0.2 to 1.2 dB peak-to-peak over the bandwidth. Additional postflight testing on the ground showed that vibrating the connecting cable between the antenna and the test equipment would produce similar results. This cable was subsequently secured to prevent reoccurrence of this effect. Since the higher change was observed during a banking turn, some reflection return from the ocean surface could have been influencing the measurements, particularly at the 500-ft measurement altitude.

The functional test flights were held during August 1982. Since the purpose of these flights was to determine the ability of the UHF radiometer to accurately measure open-ocean-surface salinity, the tests were conducted over areas where ships would be making sea-truth measurements of sea-surface temperature and salinity. To accomplish this, the test flights were coordinated with a warm core ring experiment sponsored by the National Science Foundation. Therefore, two test flights conducted on August 19 and 20, 1982, were over an area of a warm core ring where research ships were collecting sea-truth data with which the UHF radiometer data could be compared.

In addition to the UHF radiometer system on the P-3 aircraft as shown in figure 16, infrared (Barnes Engineering Co. PRT-5), L-band and C-band (SFMR) radiometers were also flown on the test flights. The onboard UHF radiometer control and data electronics rack is shown in figure 17. The UHF radiometer antenna, mounted in the forward bomb-bay section of the P-3 aircraft, is shown in figure 18. On August 19, 1982, a test flight was flown over a warm core ring area southeast of Norfolk, Virginia. A star pattern was flown over the area at an altitude of 500 ft. The aircraft passed over the Research Vessel (R/V) Endeavor from the University of Rhode Island several times. On the transit to and from this area the plane overflew the R/V Holton from Old Dominion University, which was also collecting sea-truth data. Although all frequency channels initially showed RFI, the 680-MHz channel with a 10-MHz bandwidth was selected for use, as it seemed to have the least amount of RFI

at that time. However, even though the L-band radiometer collected good data, the UHF radiometer data were useless because of RFI. On August 20, 1982, a second flight was made in an attempt to obtain RFI-free data near a ship collecting sea-truth data. Prior to this flight, an additional narrowband (10-MHz) filter was added to the 680-MHz channel. Also, the second flight was to be further out to sea over the R/V Oceanus from the Woods Hole Oceanographic Institution. It was anticipated that the greater distance at sea would provide a region free of RFI. However, the data obtained during this flight, even at a distance from land of over 200 n.mi. (370 km) were also influenced by RFI.

Summary of Results

As a result of the laboratory and flight tests of the radiometer developed for use at 500- to 710-MHz, the following observations were made:

(1) The RFI problem, mainly from UHF television stations and military communication networks, was much more severe than originally anticipated. Even with the use of multiple channels and bandwidth selection capability, the radiometer could not escape the effects of RFI to allow salinity measurements to be made during the test flight.

(2) The cold-load—antenna radiometer calibration technique in the laboratory introduced significant uncertainties. In addition to the ever-present RFI, multiple reflections caused by the physical separation between the cold load and the antenna also affected the indicated baseline brightness temperature. Also, the large physical dimensions of the cold-load—antenna interface made it difficult to maintain the cold load at a constant temperature. The resulting variations (from RFI, physical coupling, and temperature instability) were larger than had been previously experienced when this technique was used for calibrations at higher radiometer frequencies. These multiple-reflection effects are serious enough to warrant further study.

(3) The sky antenna, which was restricted to a single element by the allowable mounting space on top of the aircraft, had too broad a beamwidth and was influenced by radiation from the horizon.

(4) The high-return-loss nature of the phased-array antenna could introduce brightness temperature error if it experienced change during the vibration of flight conditions. As the flight test performed to measure this may have been influenced by cable movement and surface reflection, this test should be repeated under more controlled conditions.

(5) An RFI-free channel must be found if the UHF radiometer is to be useful for remote sensing. A test flight must then be made to verify that the new UHF channel is free of RFI and usable.

NARROWBAND SINGLE-FREQUENCY RADIOMETER DEVELOPMENT

Since RFI was the major problem associated with developing an operational UHF radiometer, it was decided to reconfigure the radiometer to operate in a single but protected RF band. As the frequency band of 608 to 614 MHz is set aside as a protected radio astronomy band, the radiometer was changed to operate at the single fixed frequency of 611 MHz with a ±3-MHz RF bandwidth. Consequently, a decrease in sensitivity had to be accepted because of the smaller RF bandwidth (6 MHz).

Therefore, the UHF radiometer operations under these restrictions would not be capable of making precision measurements of sea-surface salinity. However, because of its wavelength, the UHF radiometer might be capable of measuring other geophysical parameters such as soil moisture and even possibly penetrating vegetation cover and thereby have an advantage over other soil moisture microwave radiometer operations at L-band (1.4 GHz). Therefore, a flight testing program involving soil moisture and/or variable terrain measurements in conjunction with the Langley pushbroom (PBMR) L-band radiometer system was planned.

Receiver Redesign

The UHF receiver was redesigned to operate at 611 MHz, as shown in figure 19, by (1) replacing the input broadband (500- to 710-MHz) RF filter with an RF filter tuned to 611 MHz (±3 MHz) and (2) replacing the switchable RF band-pass filters with another 608- to 614-MHz filter.

Antenna Retuning

As the antenna was now only required to operate at a single frequency of 611 MHz, a matching network was designed and connected to the antenna phased-array output to provide a much lower VSWR match for the receiver input. The results of the retuned antenna are shown in figure 20.

Cold-Load Tests

Data from the wideband cold-load tests previously discussed were used to determine the antenna loss. The antenna loss at 611 MHz, including the loss of the matching network, was determined to be 1.77 dB. The receiver was tested with a precision coaxial cold-load termination, and the results indicated that the sensitivity at the 6-MHz bandwidth was 0.5 K for a 1-sec integration time. The calculated sensitivity for this bandwidth was 0.53 K. Also, stability tests performed over a 2-week period indicated a repeatability of calibrations within 0.5 K, which compares with the receiver sensitivity itself.

Sky Measurements

The sky antenna, as previously discussed, had a beamwidth which was too large to restrict the field-of-view to the sky. Therefore, instead of trying to design a narrower beam antenna, it was decided to make sky temperature measurements at 611 MHz and attempt to model the microwave sky background temperature at 611 MHz. Also, as the primary geophysical measurement was now to be soil moisture (i.e., an earth target instead of the sea surface), the contribution of reflected background temperature would be greatly reduced because of the much lower reflectivity of terrain compared with water surface.

Preliminary sky measurements and RFI scans were made during the winter and spring of 1983 with the 611-MHz radiometer receiver and the 30-ft dish antenna facility adjacent to Building 1299 at the Langley Research Center (LaRC). Four bow-tie elements of the type used in the phase-array antenna were used as the feed elements for the 30-ft parabolic reflector and are described in reference 12. However, since extremely long RF cable lengths had to be used between the antenna and the receiver

and their associated losses could not be maintained as a constant temperature, accurate sky temperature measurements could not be obtained. The obtained measurements did allow for an approximate measurement of brightness temperature variations over a 24-hour period, which was useful in planning the more accurate measurements later with the phased-array antenna. Also, by virtue of the steerability of the 30-ft dish, RFI scans were made on a timely basis to investigate RFI at 611 MHz. It was noted that, periodically, RFI in the form of varying-amplitude pulses was observed on a spectrum analyzer from 400 to 700 MHz. The RFI seemed to emanate from the Driver, Virginia, area. However, this form of RFI subsided by early summer, so the phased-array measurements were initiated.

Sky temperature measurements using the calibrated 611-MHz radiometer system with the phased-array antenna tuned to 611 MHz were initiated in July and continued into September 1983. The measurements for the most part were made at LaRC in an area behind Building 1299 with the UHF radiometer system in an inverted position in its transportation cradle, so that the antenna was in a zenith-viewing position. The electronics were mounted in an electronic relay rack inside a small instrumentation trailer adjacent to the radiometer system cradle. In September this setup was transported to an area near the Great Dismal Swamp National Wildlife Refuge, which was to be the area of the overflight tests, and measurements were made. A photograph of the test setup at the Dismal Swamp area is shown in figure 21. An example of the obtained sky brightness temperature for a 24-hr period is shown in figure 22. A composite of all the zenith sky temperature measurements during August and September is shown in figure 23 as a function of celestial right ascension. Also shown is a theoretical model obtained by frequency scaling data at 400 MHz from reference 13 and at 33 GHz from reference 14. As can be seen in figure 23, the comparison between the obtained results and the calculated model was good. The major difference between the results and the model was that the model showed brightness temperatures biased higher by about 5 K for the initial 6-hr period. However, based on the obtained results, the sky background brightness temperature could now be estimated within 2 K for any time over a given 24-hr period for any month of the year. For the measurement of Earth terrain, the resulting background sky reflection error would then be less than 0.5 K.

Flight Tests

Two flight tests were performed in October 1982 as preliminary steps to the redesign of the UHF radiometer at 611 MHz. First, on October 20, 1982, a test flight was conducted to insure that RFI-free operation would be possible in the 608- to 614-MHz band. Second, on October 21, 1982, an antenna VSWR test flight was made to determine if flight vibration could cause the variation of the phased-array load VSWR presented to the receiver, especially at 611 MHz. The previous flight test results, as discussed earlier in this report, were found to be inconclusive.

Figures 24(a) and (b) show the combined test setup to make the measurements for both flights, and figure 25 is a photograph of the test instrumentation. As can be seen in figure 24(a), RFI was measured with three UHF antennas: the phased-array antenna in the nadir-viewing position, the broadbeam sky antenna mounted on top of the aircraft, and a similar single-element bow-tie broadbeam antenna on the bottom of the aircraft. Also, the RFI was measured over two bandwidths. The first or broadband measurement used the original receiver 500- to 710-MHz input band-pass filter connected to the spectrum analyzer through a low-noise amplifier. This setup, similar to that of the previous RFI test flights, allowed the viewing of the total RFI spectrum for comparison. The second measurement used the two 608- to 614-MHz

band-pass filters obtained for the redesigned 611-MHz receiver and a low-noise amplifier to specifically investigate any RFI in the 6-MHz band. This test flight was flown off the Virginia/North Carolina coast at distances up to 185 n.mi. (343 km) from land and at altitudes of 500 ft (152 m) and 1000 ft (305 m). Obtained RFI results are shown in figures 26(a), (b), and (c) in photographs of the viewed RF spectrum at various points during the test flight. The pictures are grouped by type of measurement, broadband (500 to 700 MHz) or narrowband (575 to 625 MHz), and by type of antenna receiving the signal, phased-array or single-element pointing up or down. These results show that for the broadband measurements, the intensity and number of RFI signals increase with proximity to land, as expected. The RFI seems to be almost nonexistent at the greater distances from land. However, signals even barely visible on the spectrum analyzer can greatly affect the operation of the UHF radiometer because of the much greater sensitivity of the radiometer. The observed results for the narrowband channel, which was expanded to measure from 575 to 625 MHz, showed that even near land, the 608- to 614-MHz band was free of RFI. The bands of light intensity seen in the narrowband pictures are the noise band intensification from the low-noise amplifier and are restricted to 608 to 614 MHz by the filters.

On October 21, 1982, a test flight was performed over the ocean east of Wallops Island, Virginia, to measure any flight vibration effect on the phased-array antenna output VSWR which would manifest itself as an error in the observed radiometer brightness temperature. The test setup in figure 24(b) was used. Since the test cable vibration had contributed to the results from the previous test flights, this cable was secured and its vibration effect tested before and after the flight by "twanging" the cable and noting any effect on measured results. The VSWR tests during this flight were made at two frequencies. First, 650 MHz was chosen to be representative of the previous test flight frequencies (within the range of 500 to 710 MHz), and second, 611 MHz was used to test the phased array at the frequency to be used for redesign of the receiver. It should be noted that for the measurement at 611 MHz, the antenna tuning circuit was not used. The results of these tests indicated that no change in reflection coefficient (VSWR) of the phased-array antenna at either frequency any greater than the measurement accuracy of the system (0.1 dB) was observed. The only observed variations that were noted were those attributed to water-surface-reflection return at low altitude. This was noted at altitudes below 1000 ft over water and confirmed by banking maneuvers of the aircraft and flying over land/water boundaries at low altitudes.

On October 27, 1983, a functional test flight for the 611-MHz radiometer was made onboard the NASA P-3 aircraft. This test was part of a program of test flights being performed for the Langley four-beam pushbroom microwave radiometer (PBMR) L-band system. The test area overflown was that of the Great Dismal Swamp, which provides an area of variable terrain, that is, bare fields, fields with vegetation, dense forest, and freshwater boundaries. Ground-truth support was provided by personnel of the Center for Remote Sensing, U.S. Army Engineer Topographic Laboratories, Ft. Belvoir, Virginia, as part of a cooperative program. Sea-truth, offshore of the test site, was provided by the R/V Whiting, which was located near the Chesapeake Bay Bridge Tunnel. Instrument type and location in the aircraft were similar to those used on the previous functional test flights, as shown in figure 16, except that the L-band radiometer was the PBMR L-band radiometer. Also, the sky antenna was not used, as the sky measurements previously discussed enabled a background temperature correction factor to be determined for the particular time period of the overflight measurements. Sea-truth data flights over the R/V Whiting were made before and after the data flights over the Dismal Swamp area to allow for calibration of the microwave radiometers and/or comparison of inverted salinity-temperature data with brightness

temperature. Figure 27 shows the location of the obtained UHF brightness temperature for the sea-truth data for the Whiting overflights (W_1 to W_3). Also shown is a data point obtained during flights over Lake Drummond (flight lines S_1 and S_3). A comparison of the obtained data is shown in table II, where two columns of brightness temperature errors are indicated for each overflight measurement. Also indicated is the flight direction. The first column of errors σT_A^1 is derived from use of the

TABLE II.- SEA-TRUTH DATA INVERSION ERROR ANALYSIS

[Windspeed = 10.3 m/sec]

Data line	σT_A^1, K	σT_A^2, K	Flight direction
W_1	6.50	2.40	Downwind into Sun
W_2	4.10	.00	Crosswind, left side to Sun
W_3	4.20	.05	Crosswind, right side to Sun
S_1	7.60	3.90	Crosswind, left side to Sun
S_3	8.00	4.30	Crosswind, left side to Sun

laboratory cold-load calibration of the radiometer receiver. Here the brightness temperature was calculated by considering the antenna losses and computed background sky temperature and comparing the results with the expected brightness temperature as derived from the sea-truth data shown in figure 27. The errors for lines W_2 and W_3 seem to indicate a constant bias or error of 4 K in the computed brightness temperature. The error for line W_1 is 2.5 K higher (6.5 K), which may be attributed to Sun reflection bias, as this flight was downwind into the Sun, whereas lines W_2 and W_3 were crosswind with the Sun on the side of the aircraft. For the two flights over Lake Drummond, S_1 and S_3, larger errors of 7.6 and 8 K are shown. The errors for S_1 and S_3 are about 4 K higher than those for W_2 and W_3, which were flown with the same Sun orientation. As these data are for freshwater or zero salinity conditions, it is a possibility that an error of 4 K exists in the salinity algorithm for the zero value case. This explanation is substantiated by the error analysis reported in reference 10, which shows this to be a region of high data inversion error.

The second column in table II shows the errors obtained when one overflight (W_2) is used as a "bootstrap" calibration point for the radiometer, and the other overflight measurements are compared accordingly. The relative results compare favorably with the results of the first column. The W_3 line, crosswind with aircraft side to the Sun (like W_2), compares within 0.05 K. The downwind into the Sun line, W_1, shows a bias of 2.4 K, and the zero salinity overflights of S_1 and S_2 show an error of about 4 K. The wind condition for all these overflights was 20 knots (10.3 m/sec). Data from the flights over the R/V Whiting, made after the Dismal Swamp measurements, were not used in the analysis, as just prior to initiation of the first flight line, a large change in UHF radiometer brightness temperature was noted. A postflight investigation revealed that at this time, the antenna had become severely detuned because the phased-array antenna power-divider boards had separated in several locations.

The overflight lines S_1 and S_3 of the Dismal Swamp area are indicated in figure 28. These lines were planned so that variable terrain (i.e., bare fields,

vegetation, land-water boundaries, and dense forest) would be overflown on a single line. As the two flight lines S_1 and S_3 were nearly identical in location, so were the measured results, which are shown in figure 29 for S_3. Here the measured brightness temperature for the UHF radiometer and the C-band stepped frequency microwave radiometer (SFMR) is shown as a function of elapsed flight time. The UHF brightness temperature was manually offset by -50 K to separate it from the C-band data plot. Indicated on figure 29 are the regions of different terrain and individual points of response to target change. In general, the plot shows the relative insensitivity at the higher C-band microwave frequency to the difference between fields and forest, with the radiometer responding mainly to the presence of water, such as a pond or lake. In contrast, the UHF brightness temperature shows a response difference to bare fields, fields with vegetation cover, forest, and water. The UHF brightness temperature is seen in this figure to decrease for bare field conditions and increase with the presence of vegetation cover. Part of this particular flight experiment was a test to measure the ability of the onboard radiometer to penetrate the vegetation cover. For this purpose, an aluminum foil field was placed along and near the end of line S_3 on the ground at the bottom of the forest section. As the foil field is reflective, it would reflect the colder sky temperature in contrast to the warmer trees. The point indicated by E on figure 29 shows a slight dip in the received brightness temperature and indicates that the UHF radiometer did sense the foil field, but only partially. This slight response was not surprising, as this particular section of forest was dense, and the tree heights were several orders of magnitude greater than the UHF wavelength.

For the purpose of comparing the UHF radiometer response with that of the L-band (PBMR) radiometer, the response for beam no. 3 of the PBMR radiometer (also offset by -50 K) is shown in figure 30 for the same flight line (S_3). Although beam no. 3 was 8° off-nadir, the measured data are still representative of that which would be obtained at nadir. It can be seen by comparing the results of the UHF radiometer in figure 29 with those of the L-band radiometer in figure 30 that they are almost identical in terms of response to various terrain features.

CONCLUDING REMARKS

The conclusions for this development program can best be described by first summarizing the results of the UHF radiometer development effort. The prime reason for undertaking the UHF radiometer development was the fact that the derived algorithms showed that increased sensitivity is obtained in the change in observed brightness temperature corresponding to a change in sea-surface salinity at the UHF band as compared with the previously used higher L-band frequency. Therefore, theoretically, the UHF band should have been able to measure the salinity of the open ocean to the required accuracy of a fraction of 1 $^{\circ}/_{oo}$. However, the results for the UHF radiometer development show that while this may appear theoretically possible, it is not obtainable in practice.

The accuracy of the measured brightness temperature is dependent on several contributing factors being very accurately known. First, the background sky temperature, which is reflected from the water surface, is much greater and more variable over a 24-hr period at the UHF band than at L-band. The antenna losses must be precisely known and remain temperature constant, especially if they are appreciable (> 1 dB), as they were for the UHF radiometer. Also, the brightness-temperature-to-salinity inversion error is a function of the radiometer sensitivity, so that lower errors and thus improved accuracies are obtained by lower sensitivity values, which

for a given radiometer on an aircraft or other moving remote-sensing platform, are obtained by increasing bandwidth.

The single most important and critical factor, which unfortunately was initially underestimated in this radiometer development, was that of radio-frequency interference (RFI). Even though the radiometer was initially designed with many channels in the 500- to 710-MHz region with variable bandwidths (to obtain the largest bandwidth possible without RFI), the amount of RFI encountered in the eastern Virginia land and sea area of the testing program was overwhelming. Actually, this region was possibly one of the worst areas in terms of UHF television transmissions in which to try to use a UHF radiometer. No RFI-free channel could be found, even several hundred miles out to sea, in order to test the radiometer. A better test area might have been the southwest region of the U.S., but even that area, while having a much lower amount of UHF television transmissions, may have had a higher amount of UHF communication transmissions because of the large number of military airbases in that area.

The solution to the RFI problem was to redesign the radiometer to operate in the protected radio astronomy band of 608 to 614 MHz. While this proved to be successful, the consequence was that the reduced bandwidth degraded the sensitivity so severely that accurate retrieval of sea-surface salinity was not possible. However, the UHF band was believed to be useful, like the L-band region, for the measurement of soil moisture and/or terrain. It was further believed that the longer wavelength would enable the penetration of vegetation and possibly have an advantage over L-band for the measurement of soil moisture with vegetation cover. Furthermore, as the ground is not as reflective as water, the sky background contribution would be much less and therefore less susceptible to error. The flight test over the Great Dismal Swamp area did in fact demonstrate the RFI-free operation of the UHF radiometer and its ability to measure the change in terrain characteristics. However, since the flight was not over a controlled soil moisture test area, the ability of the UHF radiometer to measure soil moisture with or without vegetation cover was not tested. The slight response of the UHF radiometer to a foil field located in a dense forest section of the Dismal Swamp area was not a true test of its ability to penetrate vegetation-covered fields, as the tree heights were orders of magnitude greater than the UHF wavelength. The most notable result obtained during this test flight was that while the UHF radiometer showed good sensitivity in response to terrain change, the L-band radiometer, with its shorter wavelength, demonstrated at least equal sensitivity to the same change of terrain.

In summary, it can then be stated that the theoretical advantage of greater sensitivity at the UHF band to geophysical parameter change is more than negated by the practical problems of operations in the UHF region, mainly that of RFI. In conclusion, it seems that the L-band frequency and corresponding L-band radiometers provide a more practical measurement approach for the remote sensing of the geophysical parameters of both sea-surface salinity and soil moisture.

NASA Langley Research Center
Hampton, VA 23665-5225
August 13, 1985

REFERENCES

1. Swift, C. T.: Passive Microwave Remote Sensing of the Ocean - A Review. Boundary-Layer Meteorol., vol. 18, no. 1, Feb. 1980, pp. 25-54.

2. Blume, Hans-Juergen C.; Kendall, Bruce M.; and Fedors, John C.: Measurement of Ocean Temperature and Salinity Via Microwave Radiometry. Boundary-Layer Meteorol., vol. 13, nos. 1, 2, 3, 4, Jan. 1978, pp. 295-308.

3. Swift, Calvin T.; and McIntosh, Robert E.: Considerations for Microwave Remote Sensing of Ocean-Surface Salinity. IEEE Trans. Geosci. & Remote Sensing, vol. GE-21, no. 4, Oct. 1983, pp. 480-491.

4. Hollinger, James P.: Microwave Properties of a Calm Sea. Rep. No. 7110-2, Naval Res. Lab., Aug. 15, 1973. (Available from DTIC as AD 771 374.)

5. Ulaby, Fawwaz T.; Moore, Richard K.; and Fung, Adrian K.: Microwave Remote Sensing - Active and Passive. Volume I - Microwave Remote Sensing Fundamentals and Radiometry. Addison-Wesley Pub. Co., 1981.

6. Apinis, John J.; and Peake, William H.: Passive Microwave Mapping of Ice Thickness. Final Rep. 3892-2 (NASA Grant, NSG-3005), Ohio State Univ. Electrosci. Lab., Aug. 1976. (Available as NASA CR-149104.)

7. Shakeshaft, J. R.; and Webster, A. S.: Microwave Back-Ground in a Steady State Universe. Nature, vol. 217, no. 5125, Jan. 20, 1968, pp. 339-340.

8. Rana, N. C.: Cosmic Thermalization and the Microwave Background Radiation. Mon. Not. R. Astron. Soc., vol. 197, no. 3, Dec. 1981, pp. 1125-1137.

9. Webster, William J., Jr.; Wilheit, Thomas T.; Ross, Duncan B.; and Gloersen, Per: Spectral Characteristics of the Microwave Emission From a Wind-Driven Foam-Covered Sea. J. Geophys. Res., vol. 81, no. 18, June 20, 1976, pp. 3095-3099.

10. Britt, Charles L., Jr.: Errors in Radiometric Remote Sensing of Sea-Surface Temperature and Salinity. IEEE Trans. Geosci. & Remote Sens., vol. GE-22, no. 6, Nov. 1984, pp. 627-632.

11. Bailey, M. C.: Broad-Band UHF Dipole Array. NASA TM-86373, 1985.

12. Bailey M. C.; and Hefner, B. B., Jr.: Development of a 611 MHz Feed for a 9-Meter Reflector. NASA TM-86300, 1984.

13. Taylor, Ralph E.: 136-MHz/400-MHz Radio-Sky Maps. Proc. IEEE, vol. 61, no. 4, Apr. 1973, pp. 469-472.

14. Lubin, Philip M.; and Smoot, George F.: Polarization of the Cosmic Background Radiation. Astrophys. J., vol. 245, no. 1, pt. 1, Apr. 1, 1981, pp. 1-17.

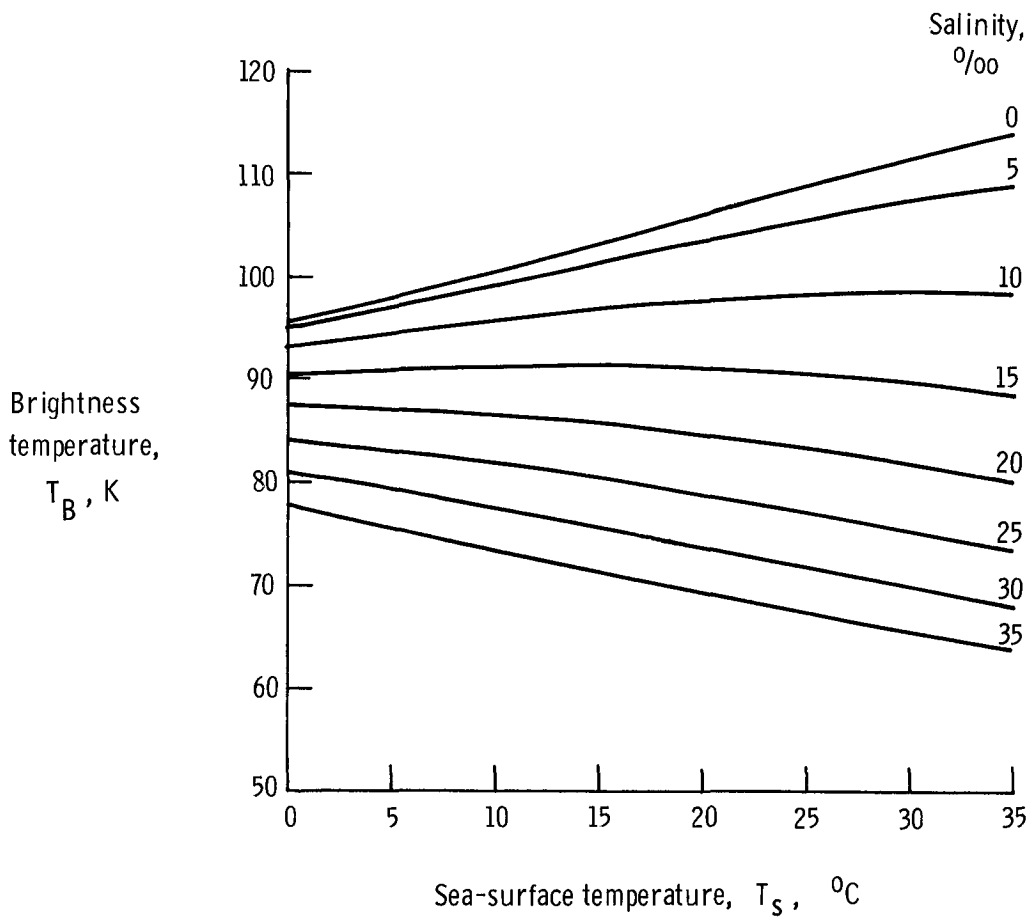

Figure 1.- Brightness temperature as a function of salinity and surface temperature at a frequency of 620 MHz.

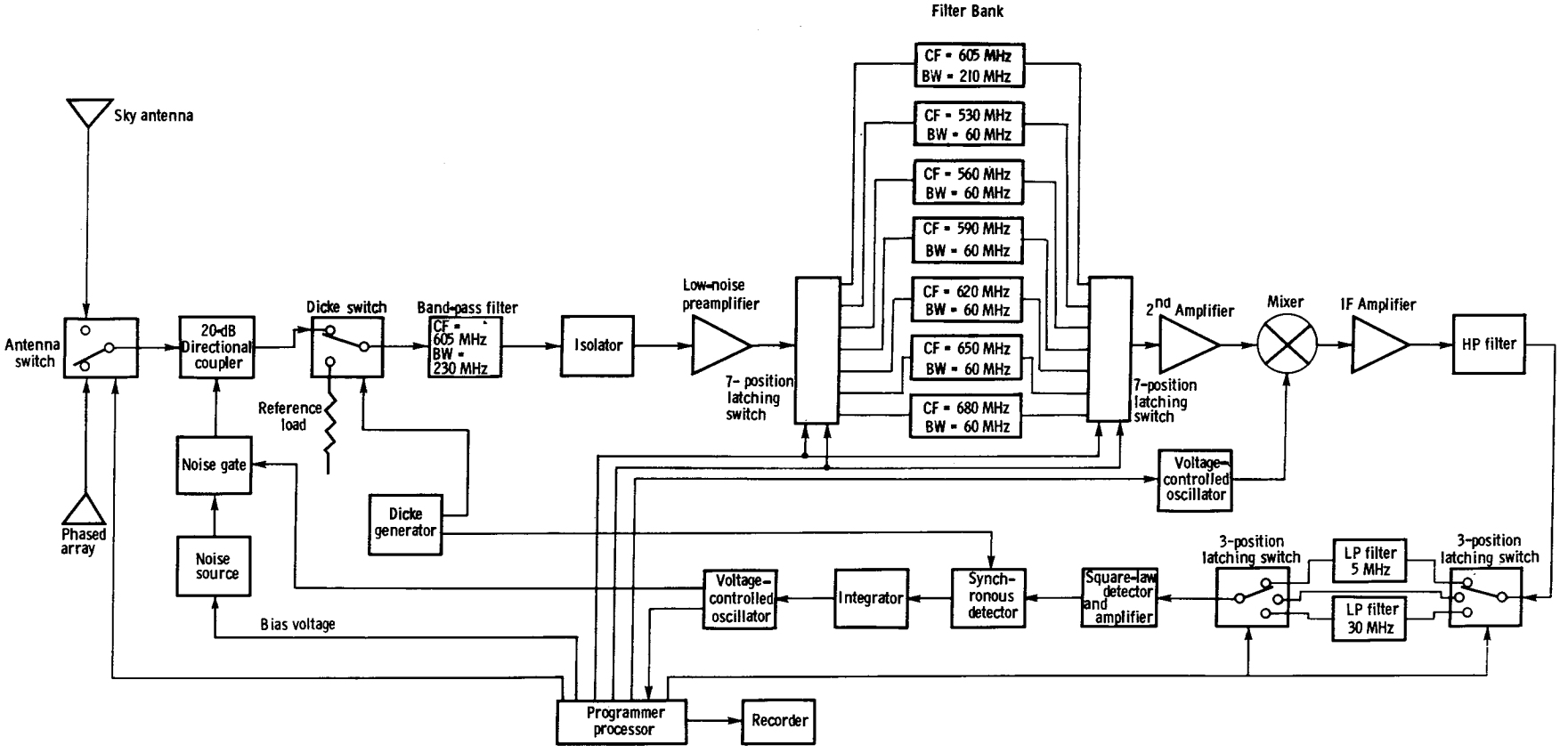

Figure 2.- UHF radiometer block diagram.

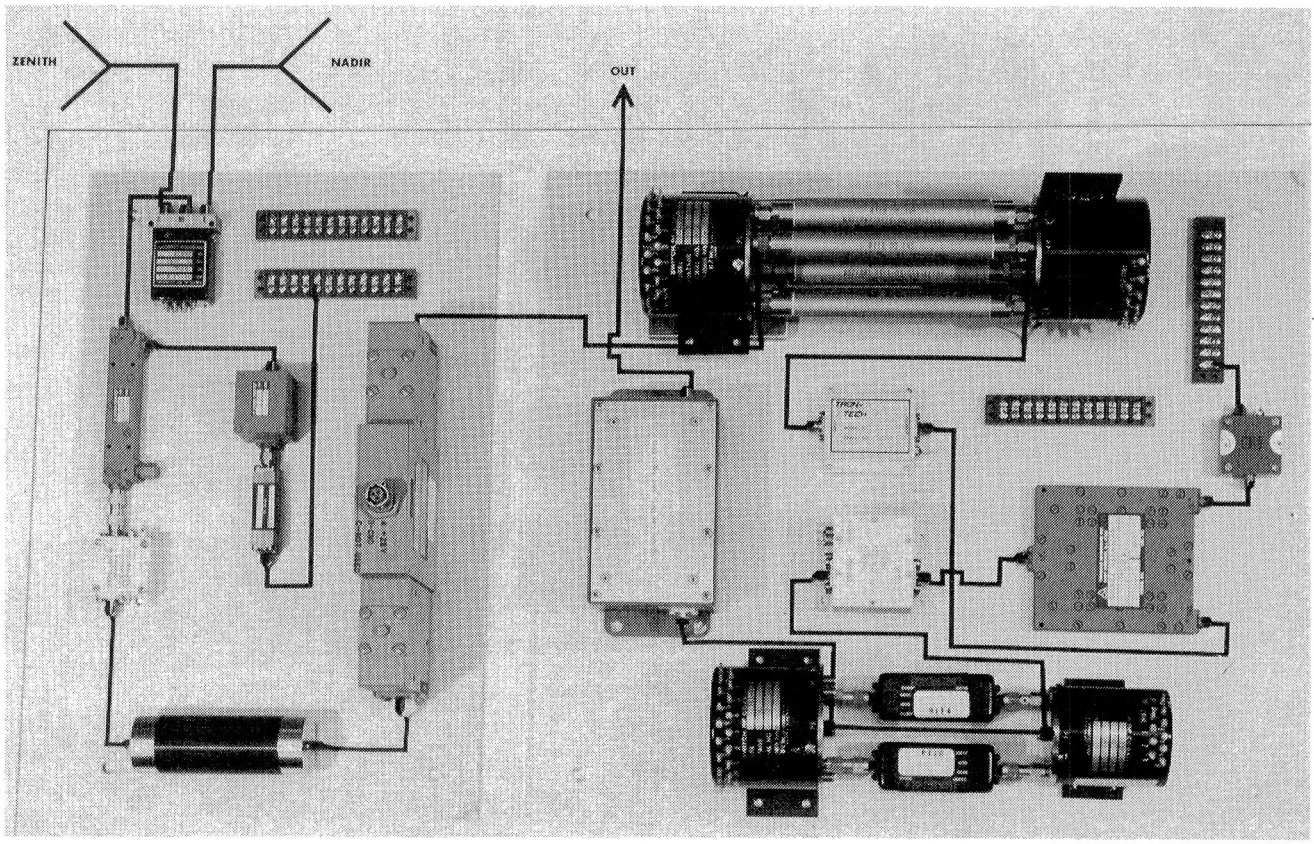

L-82-546

Figure 3.- Layout of receiver components.

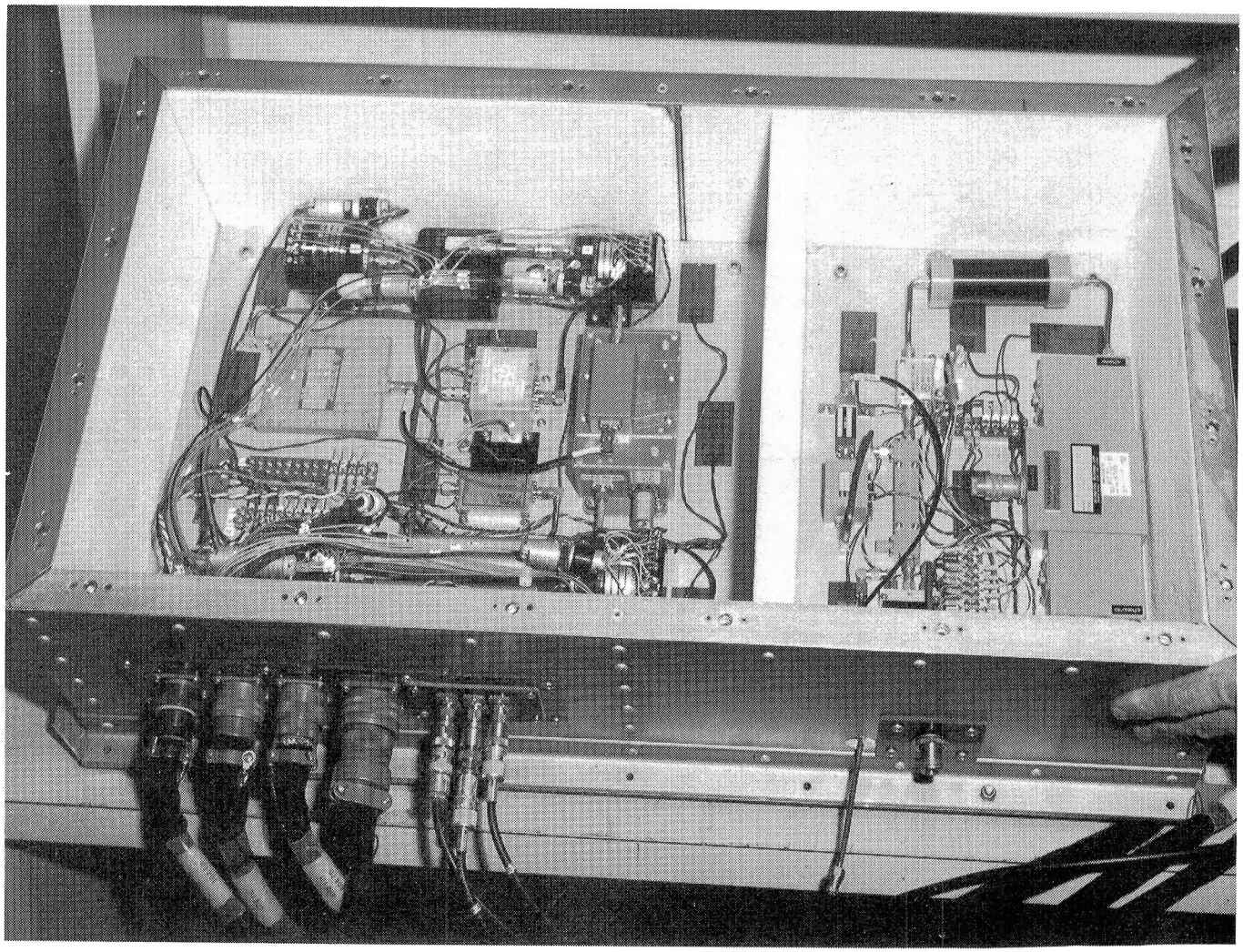

L-82-5252

Figure 4.- Thermally insulated receiver enclosure.

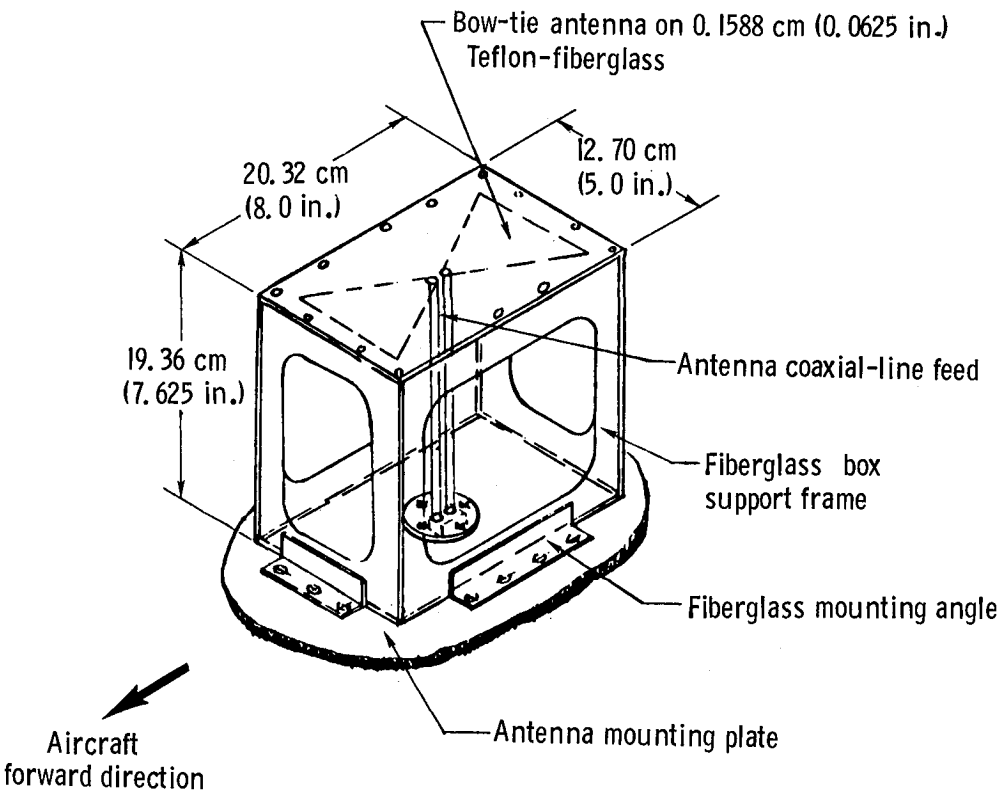

Figure 5.- UHF bow-tie antenna. (Teflon is a trademark of E. I. du Pont de Nemours and Co.)

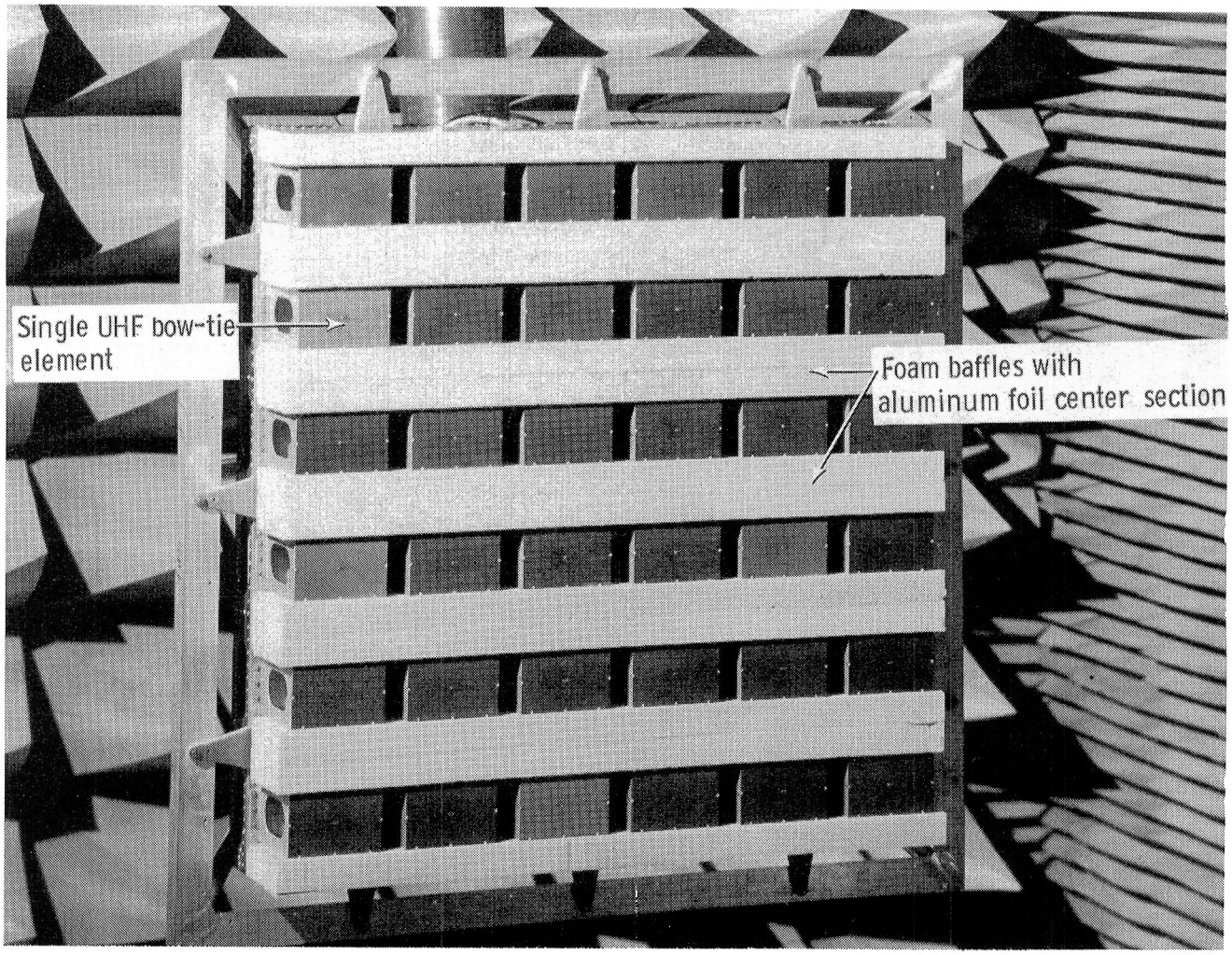

L-82-6432

Figure 6.- 6 × 6 element array of UHF radiometer antenna on mounting frame.

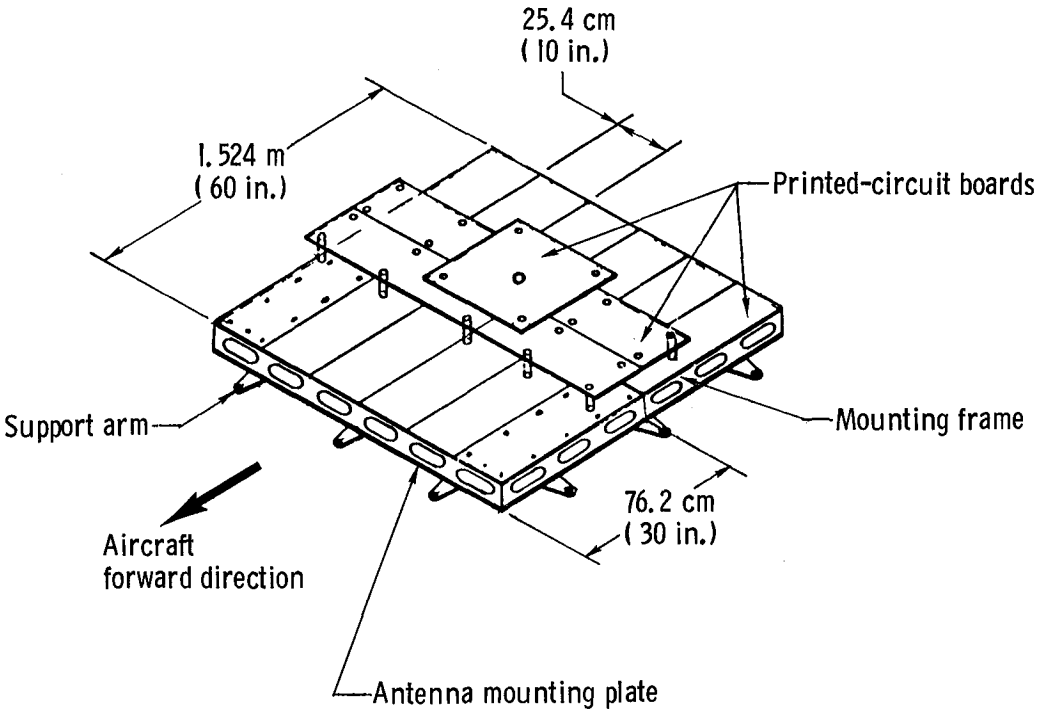

Figure 7.- Printed-circuit combining-feed configuration for UHF radiometer antenna array.

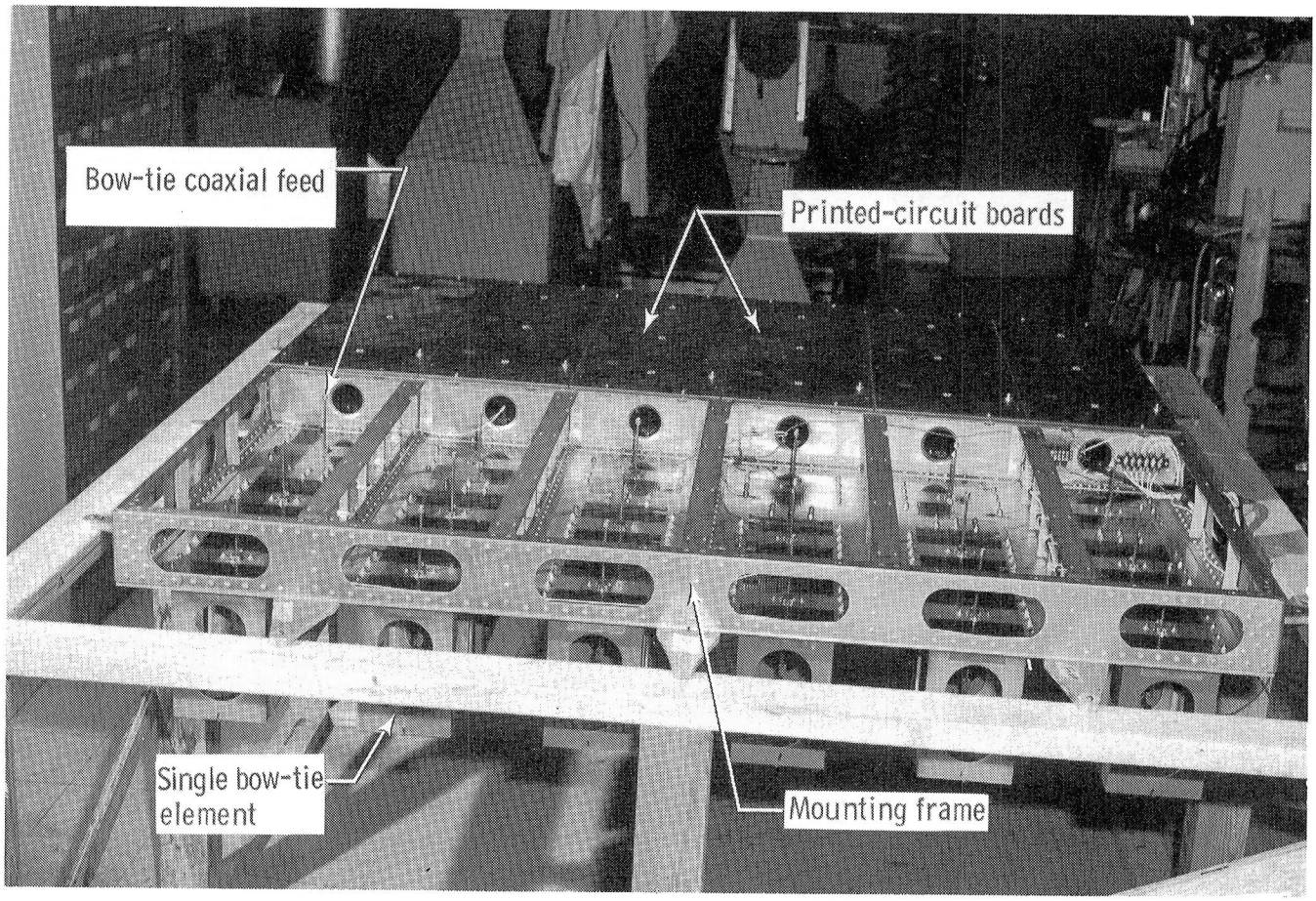

L-82-5251

Figure 8.- UHF radiometer antenna array during assembly.

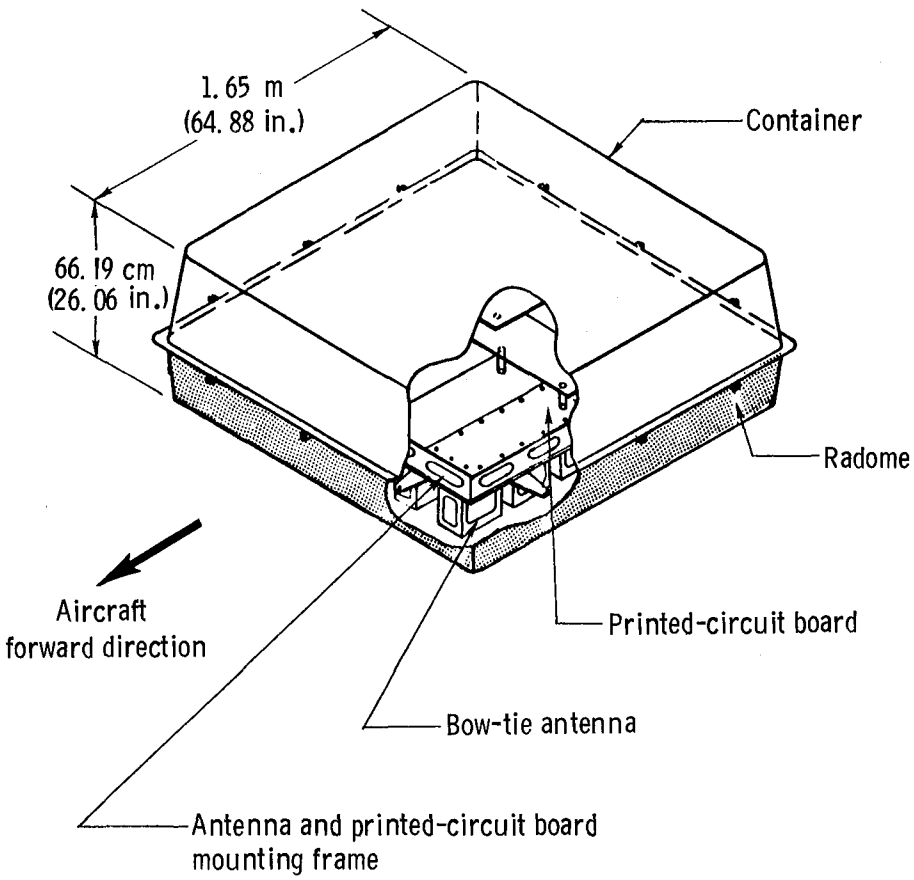

Figure 9.- Assembled UHF radiometer antenna array showing cutaway view of container.

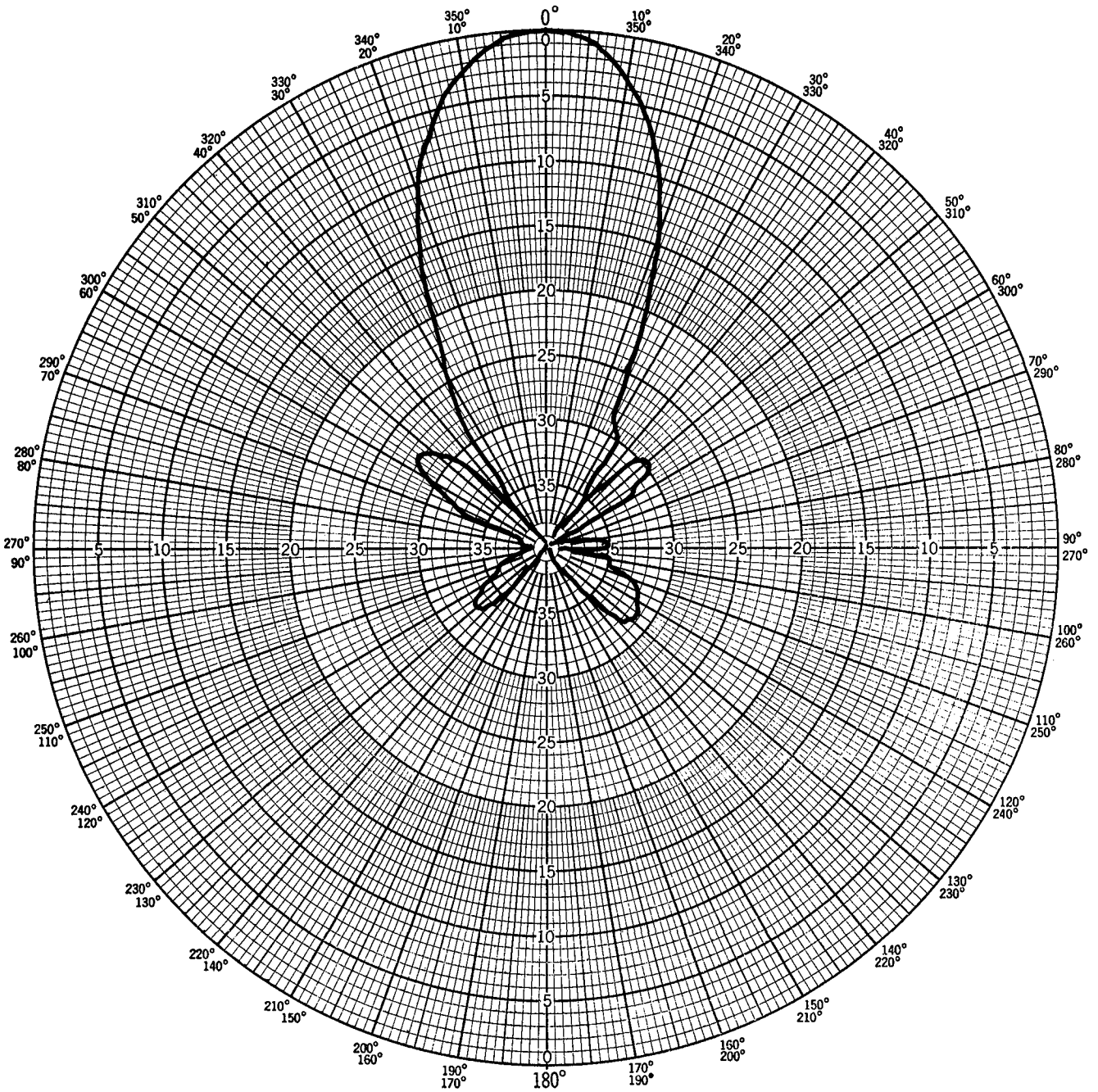

(a) Vertical polarization.

Figure 10.- Antenna radiation pattern of UHF radiometer antenna array with radome at a frequency of 620 MHz.

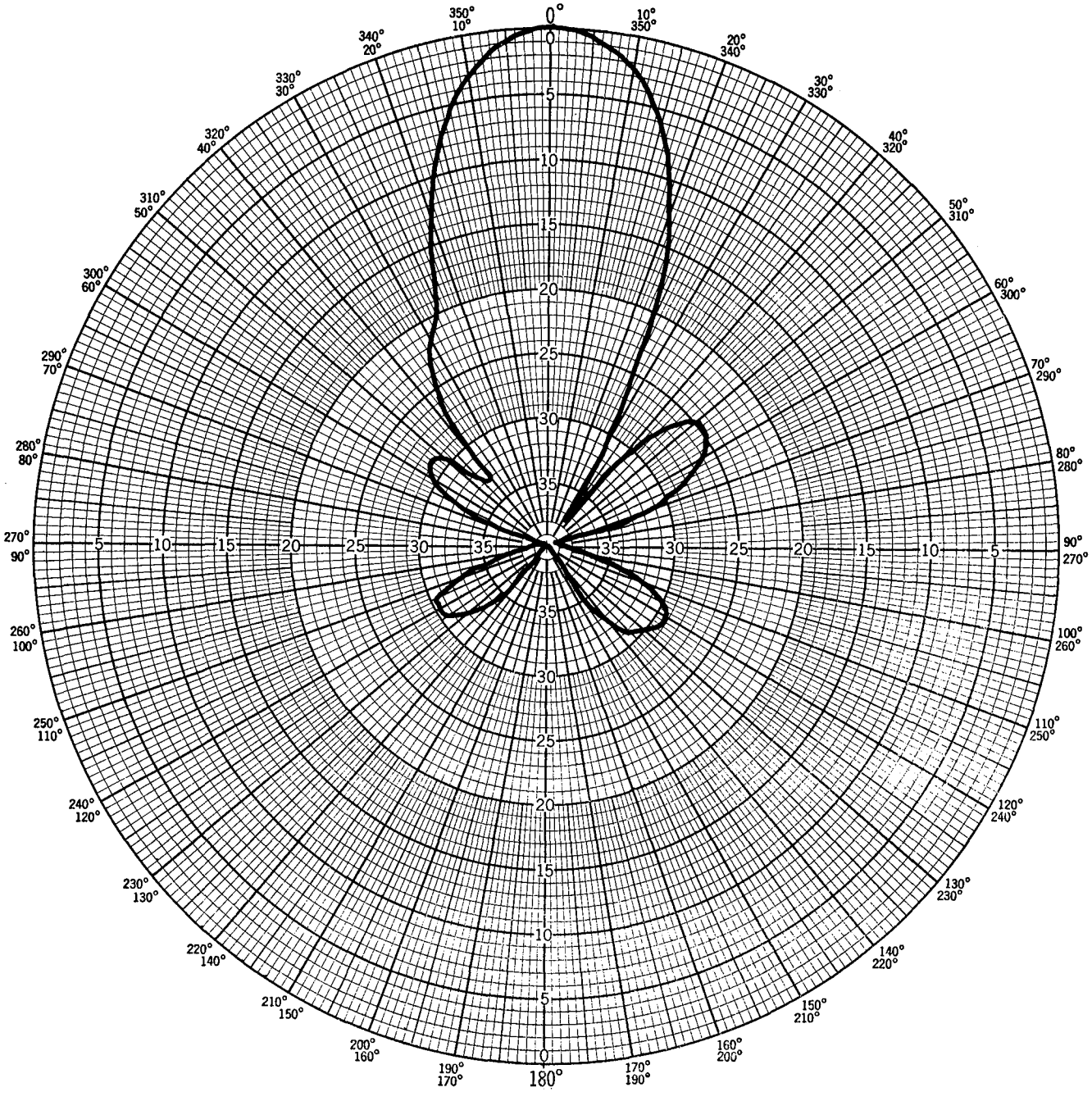

(b) Horizonal polarization.

Figure 10.- Concluded.

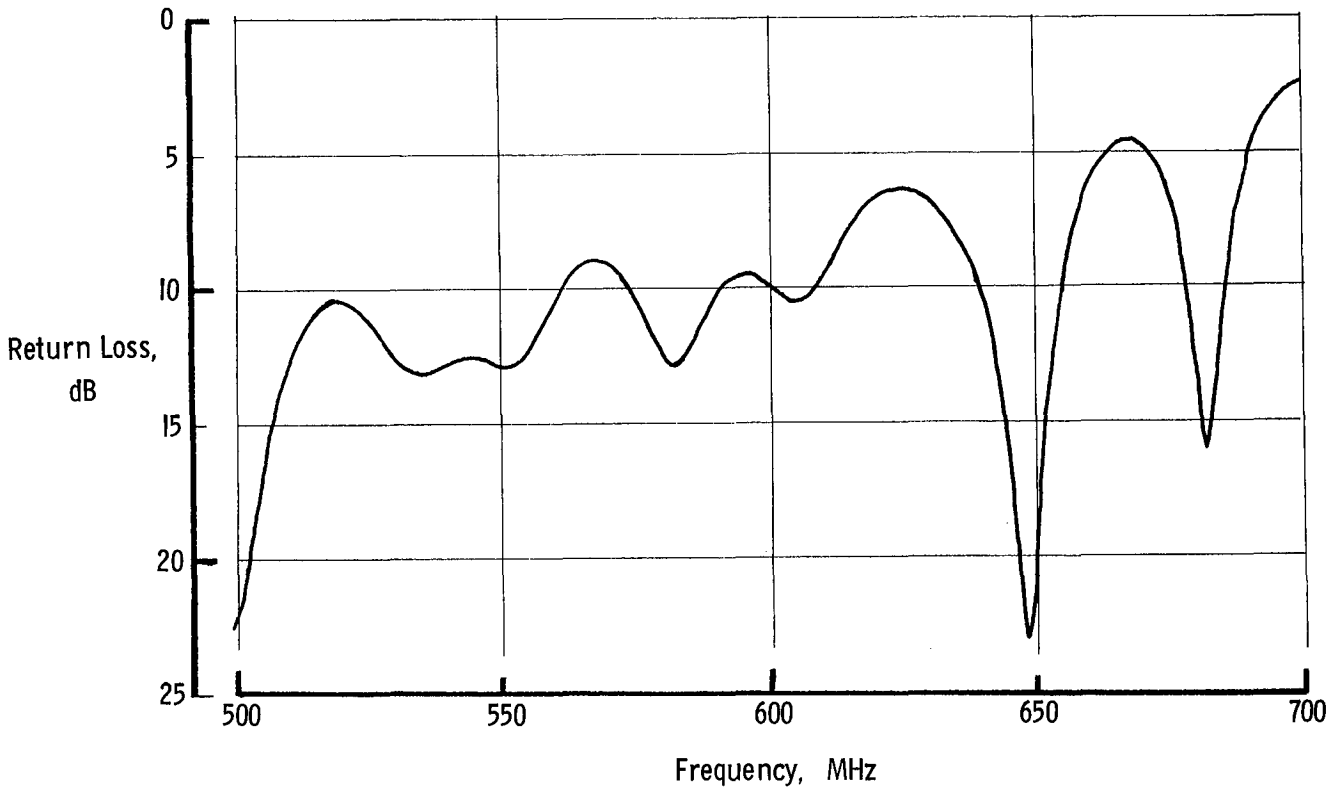

Figure 11.- Return-loss measurement of UHF radiometer antenna array in Langley Anechoic Antenna Test Facility.

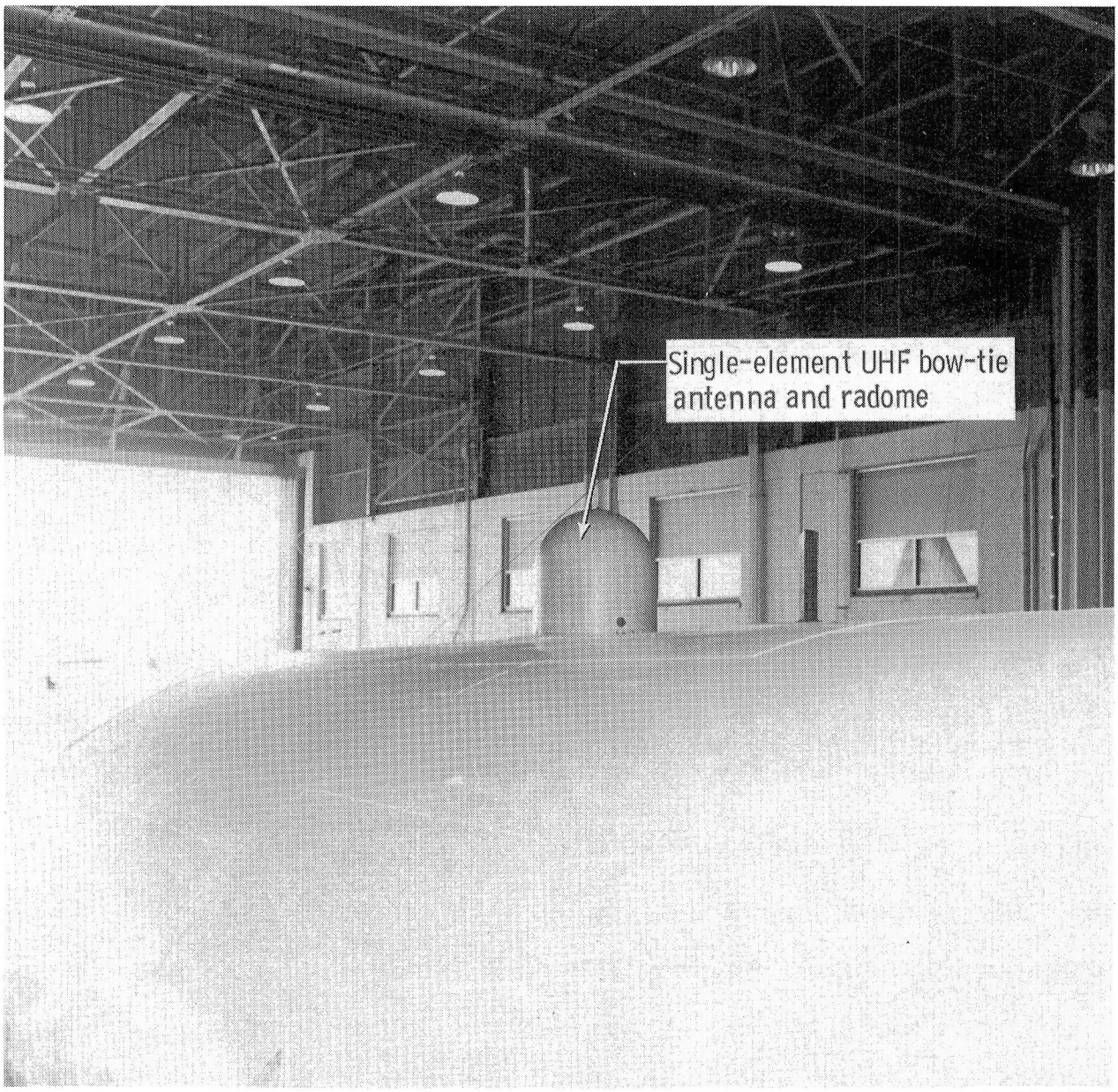

L-85-131

Figure 12.- Single-element UHF bow-tie sky antenna with radome mounted on top of P-3 aircraft.

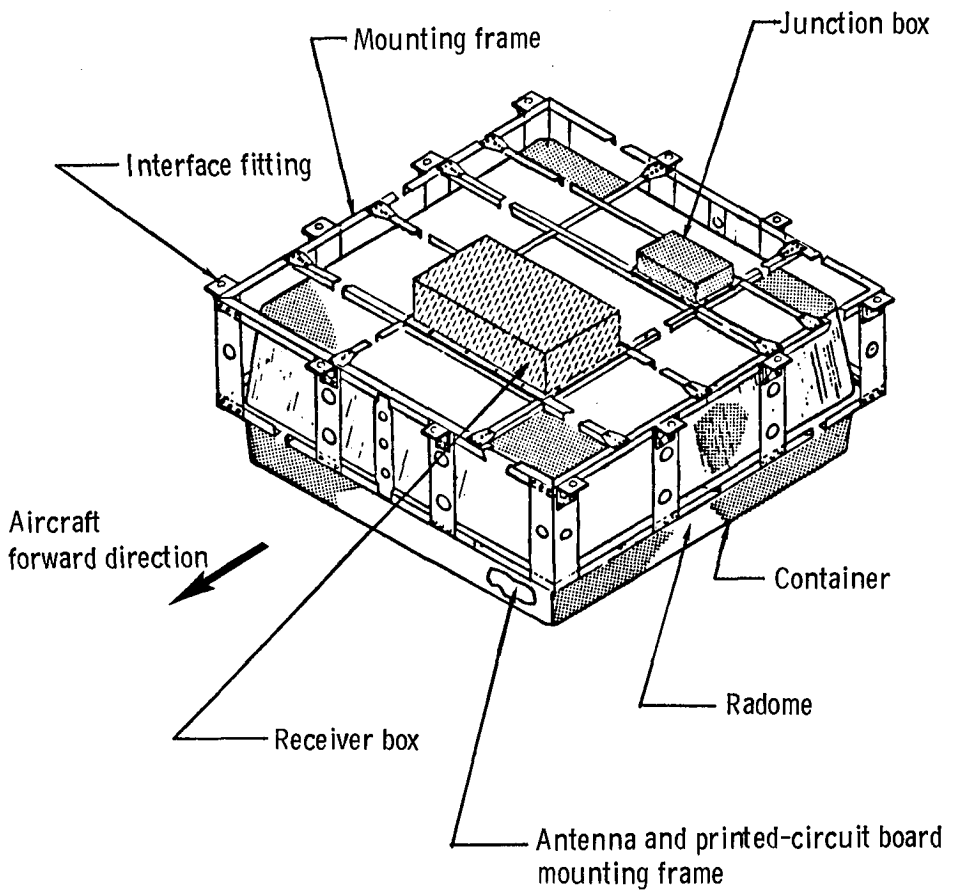

(a) Complete assembly drawing.

Figure 13.- UHF radiometer system.

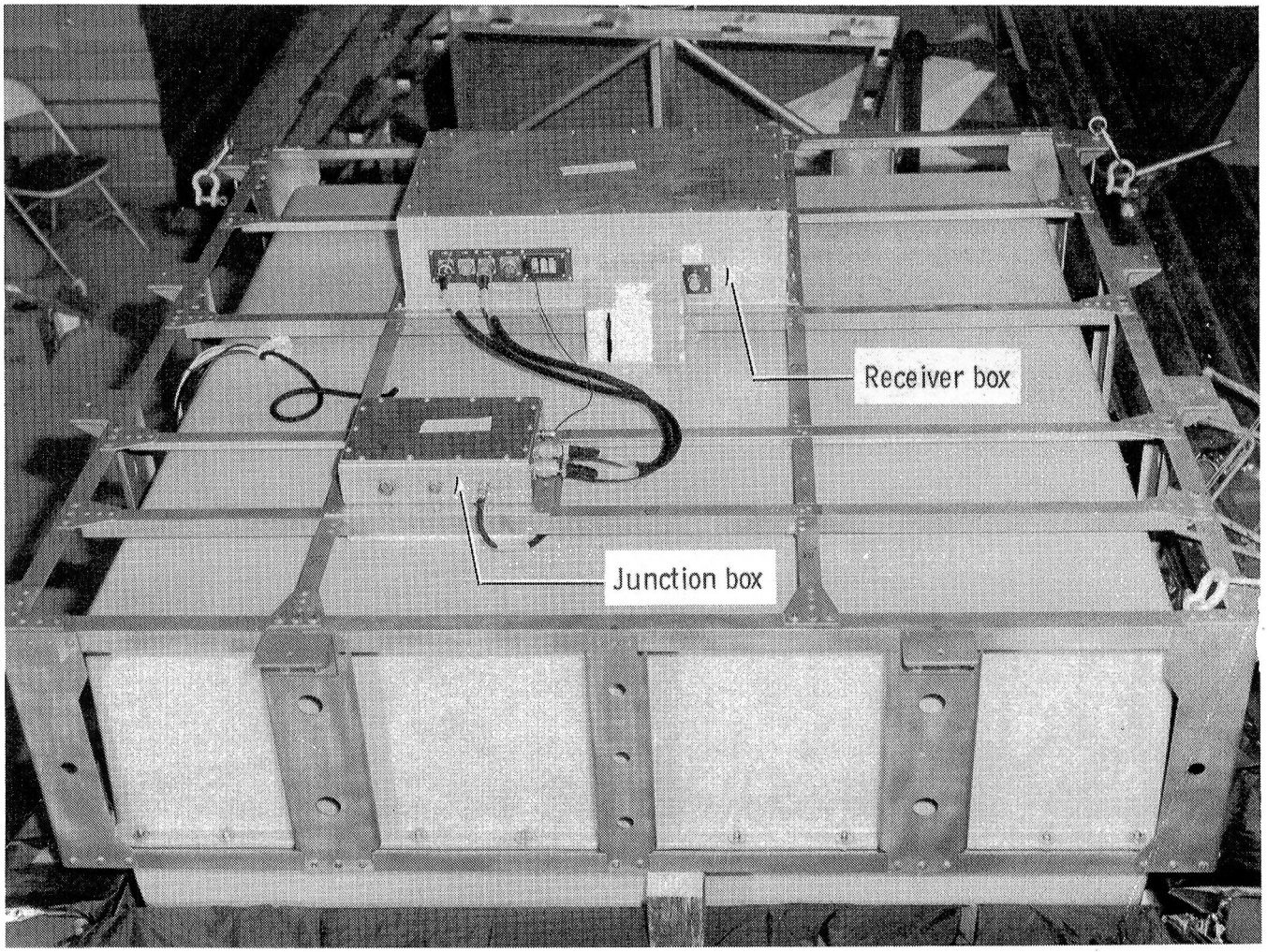

L-82-7837

(b) Photograph of assembly.

Figure 13.- Concluded.

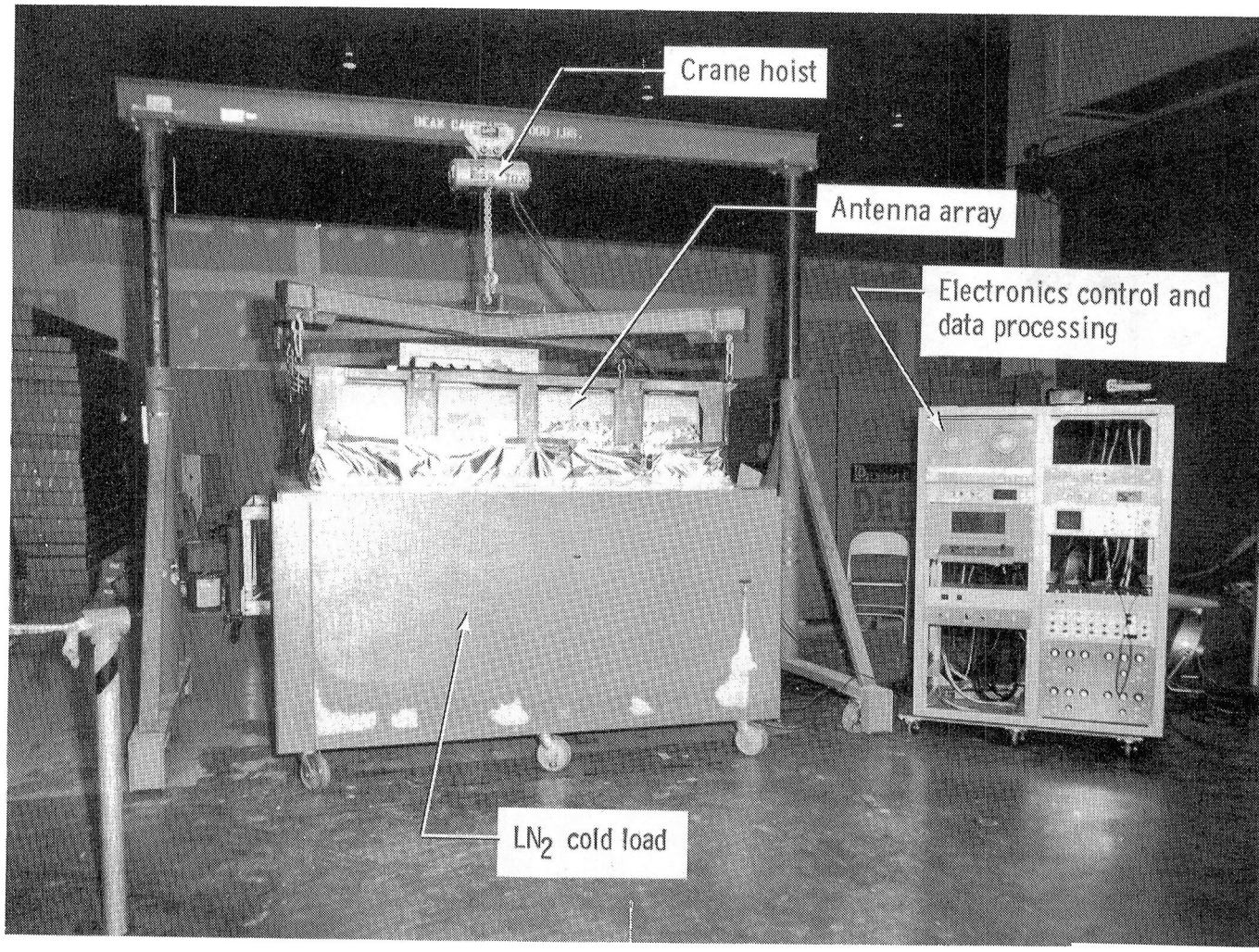

L-82-7293

Figure 14.- UHF radiometer with LN_2 cold-load test setup.

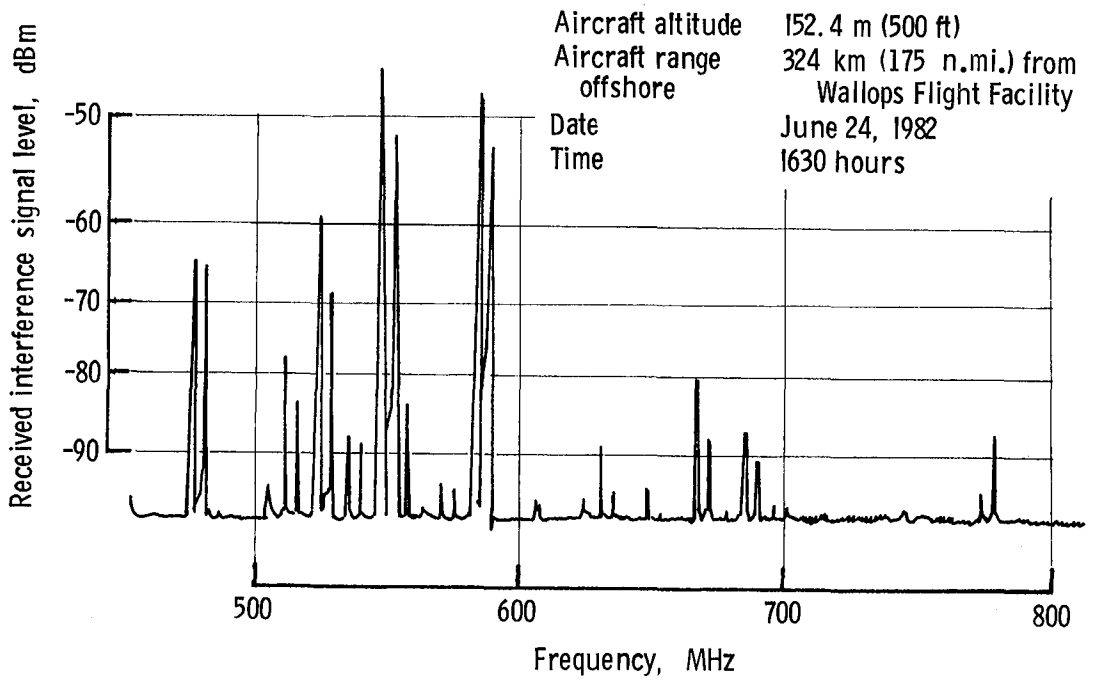

(a) Distant from Wallops.

Figure 15.- Spectral measurement of radio-frequency interference (RFI) signals received by single UHF bow-tie antenna (sky antenna) mounted below P-3 aircraft.

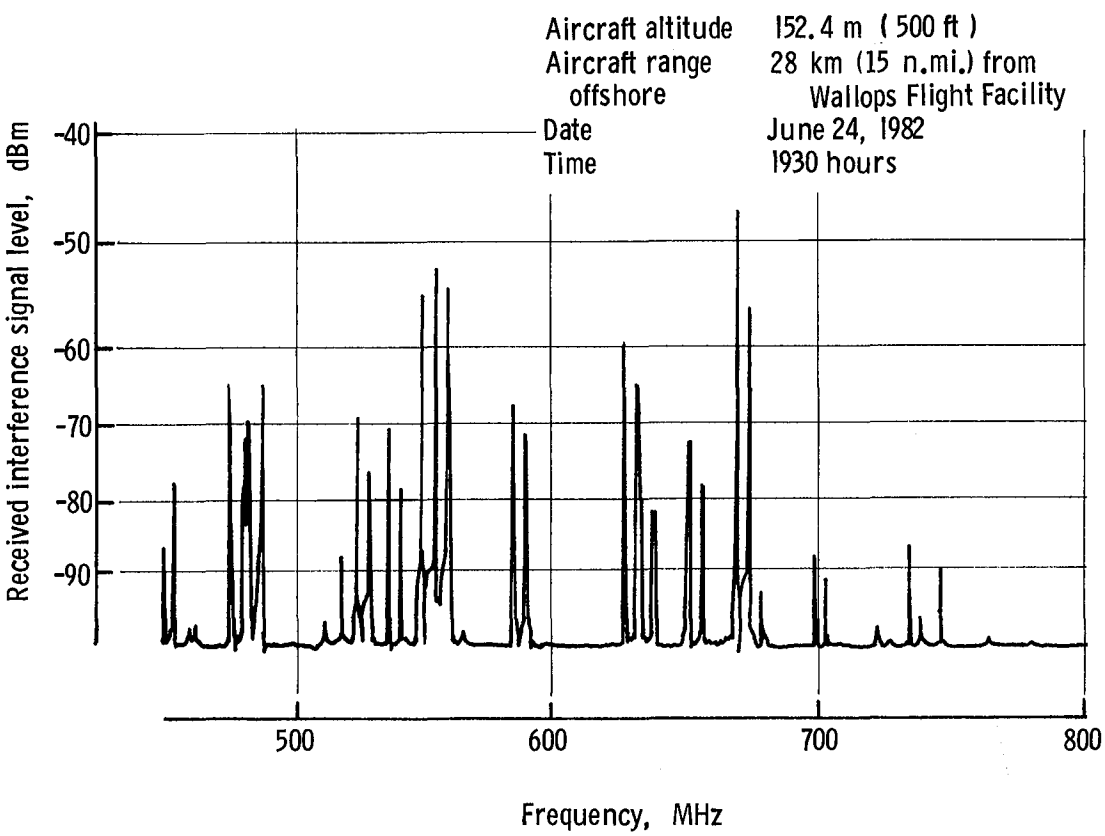

(b) Near Wallops.

Figure 15.- Concluded.

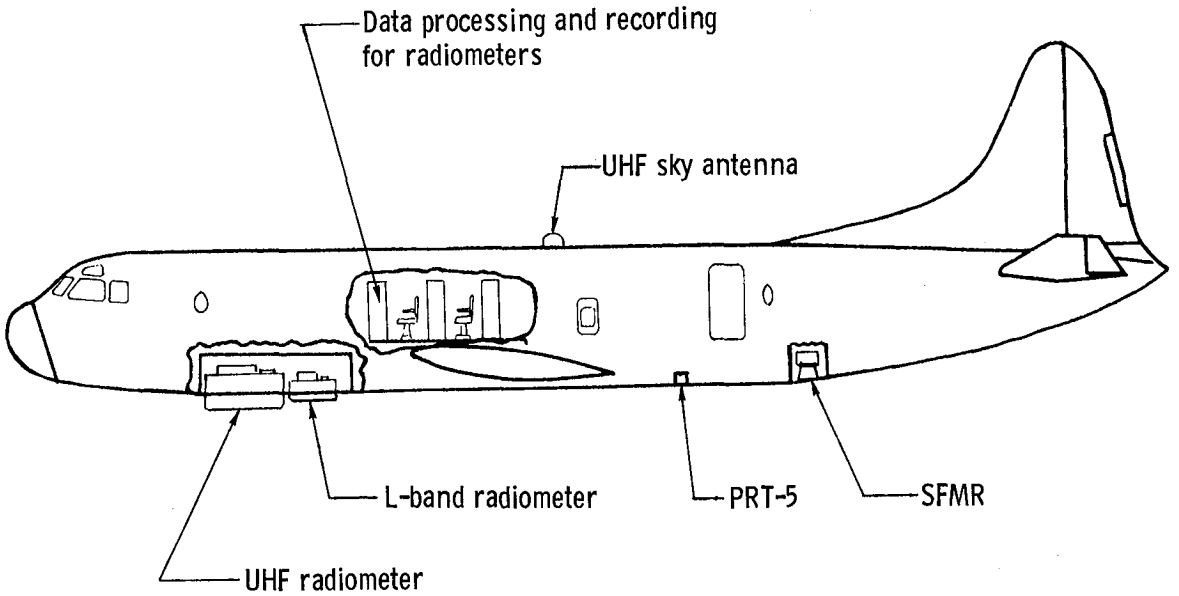

Figure 16.- Plan view of instrument package installation on P-3 aircraft for UHF radiometer testing.

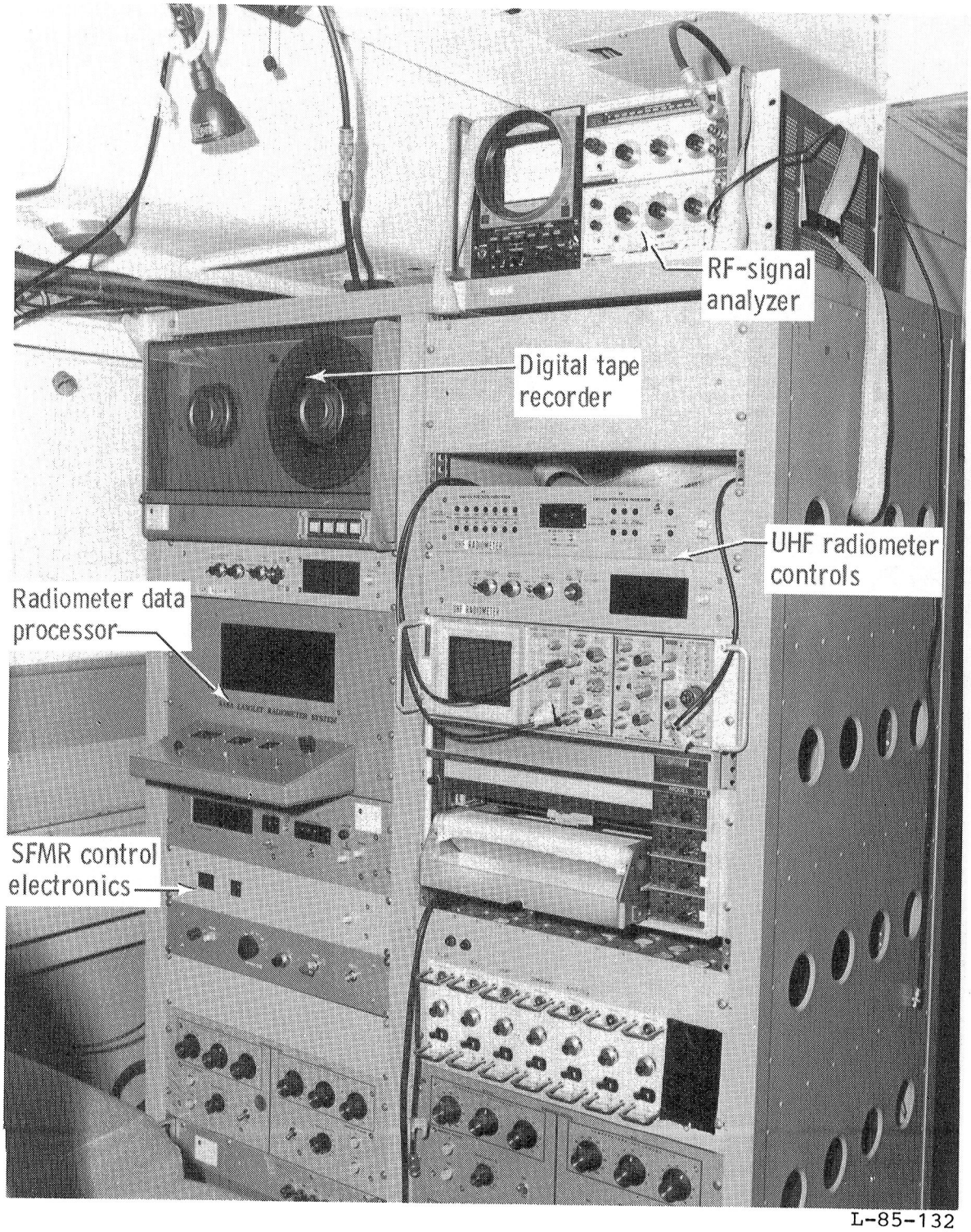

Figure 17.- Data processing and recording systems for UHF, SFMR, and L-band radiometers aboard P-3 aircraft.

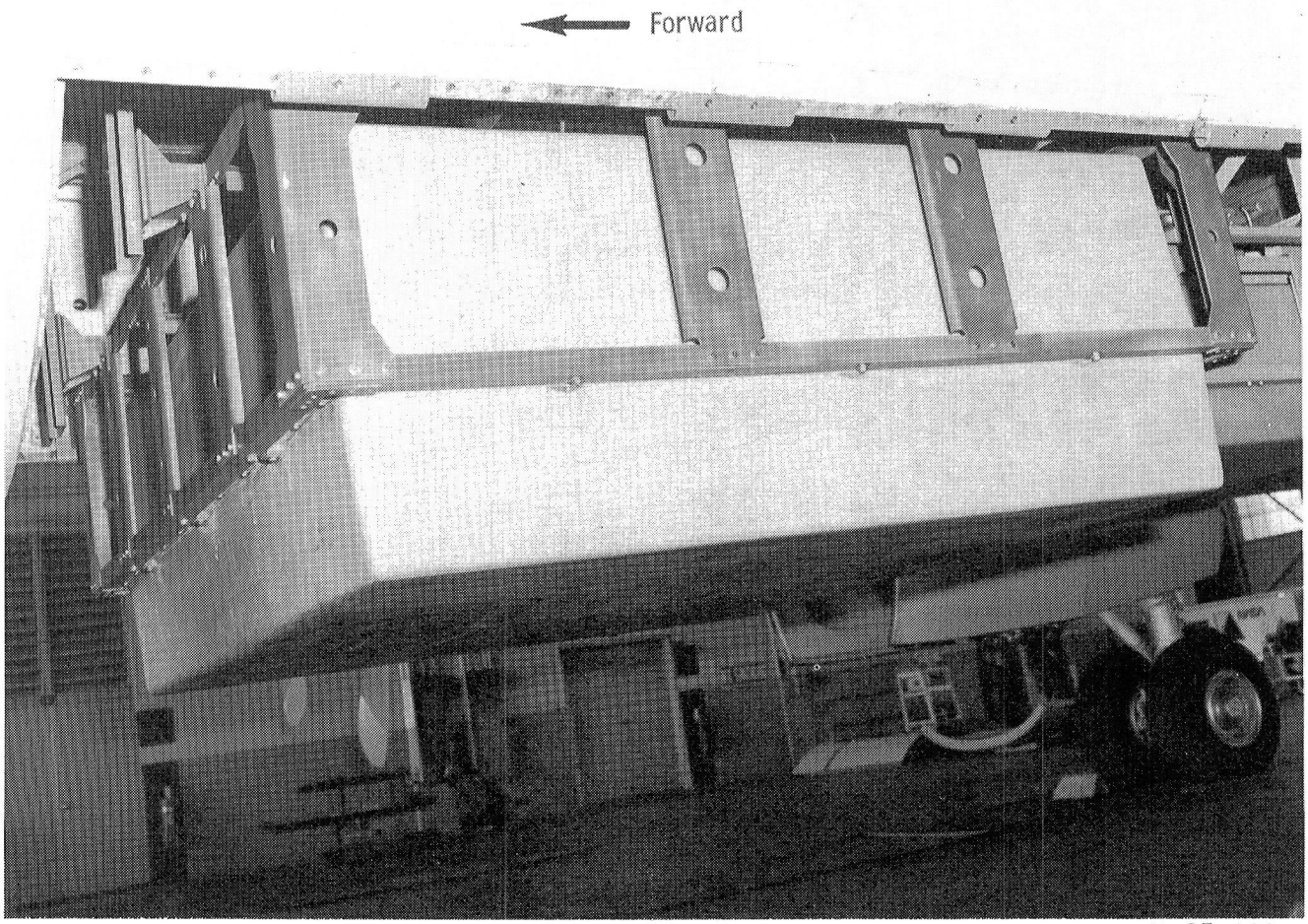

L-85-133

Figure 18.- UHF radiometer antenna array mounted in forward bomb bay of P-3 aircraft.

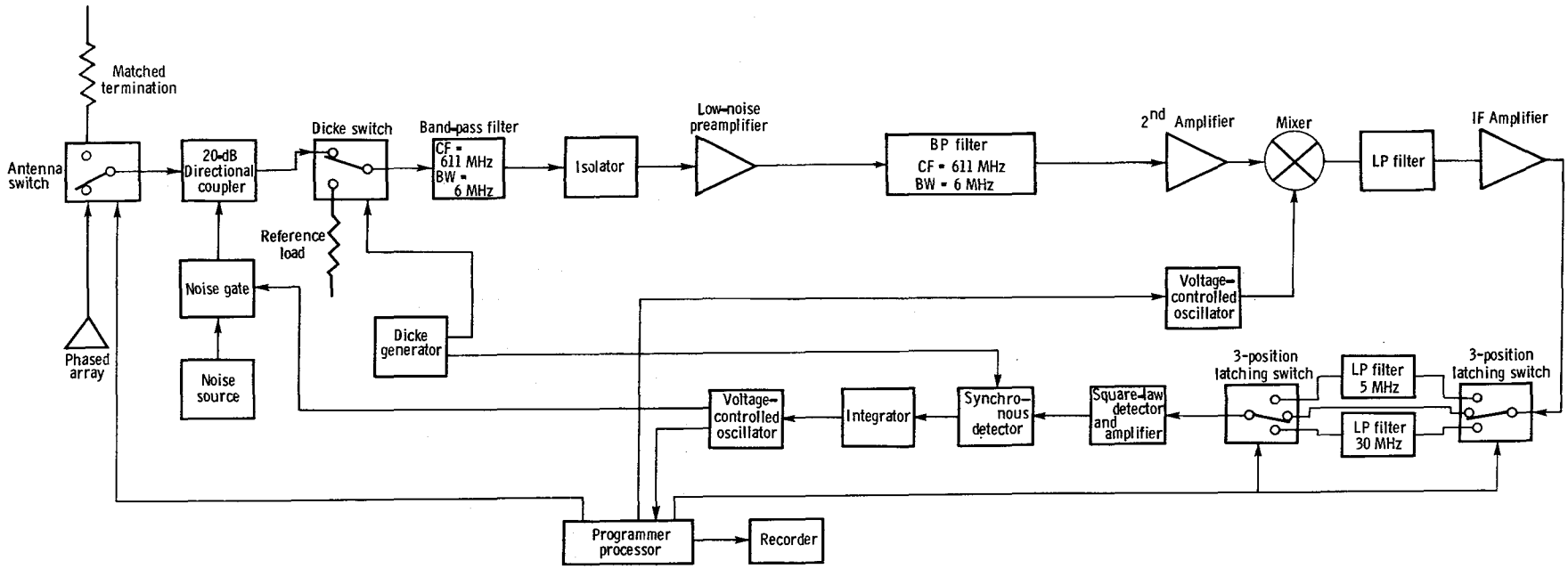

Figure 19.- Block diagram of narrowband single-frequency radiometer.

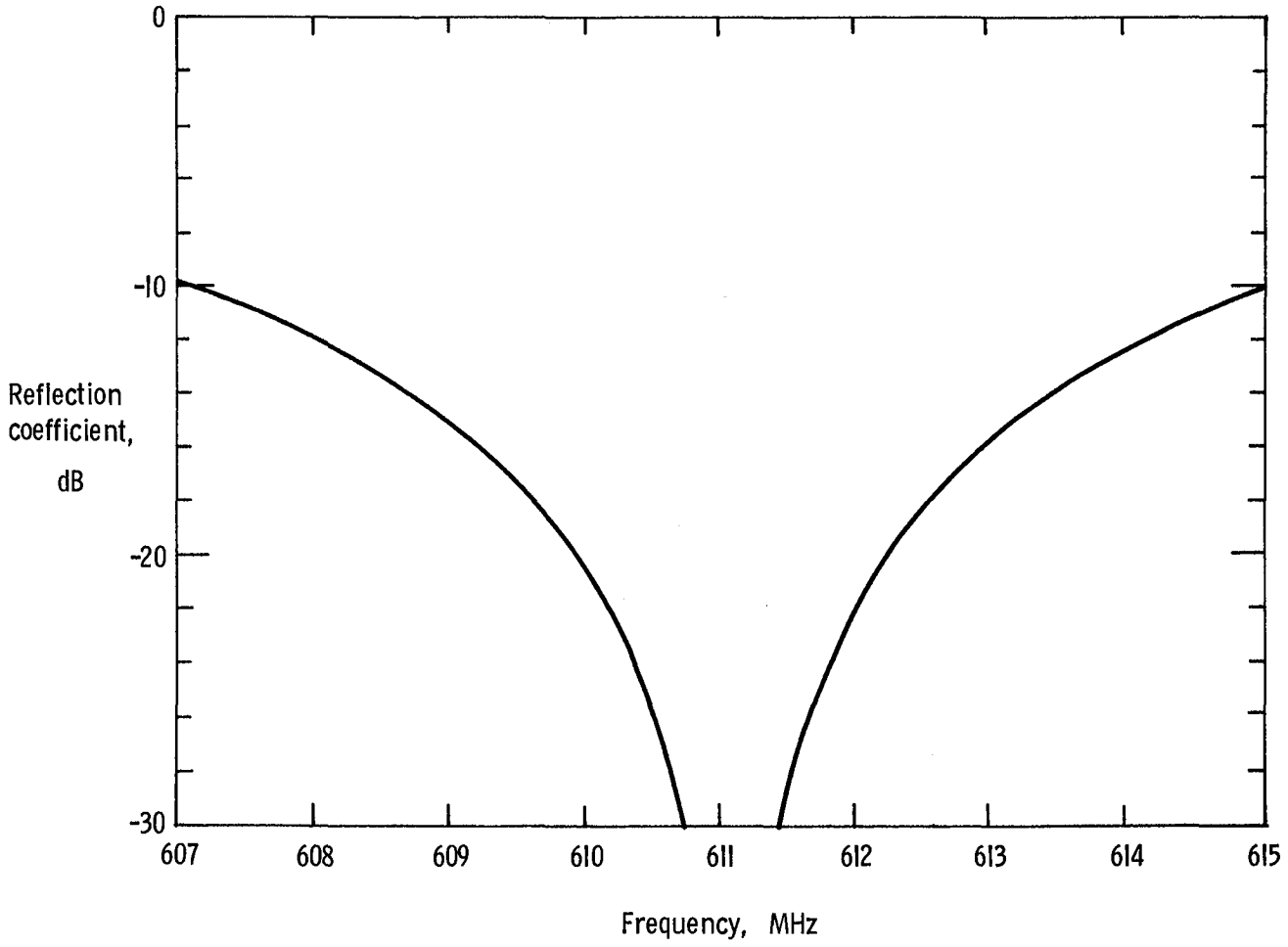

Figure 20.- Reflection coefficient as a function of frequency for UHF radiometer antenna (36-element bow-tie array). Antenna tuned for 611 MHz.

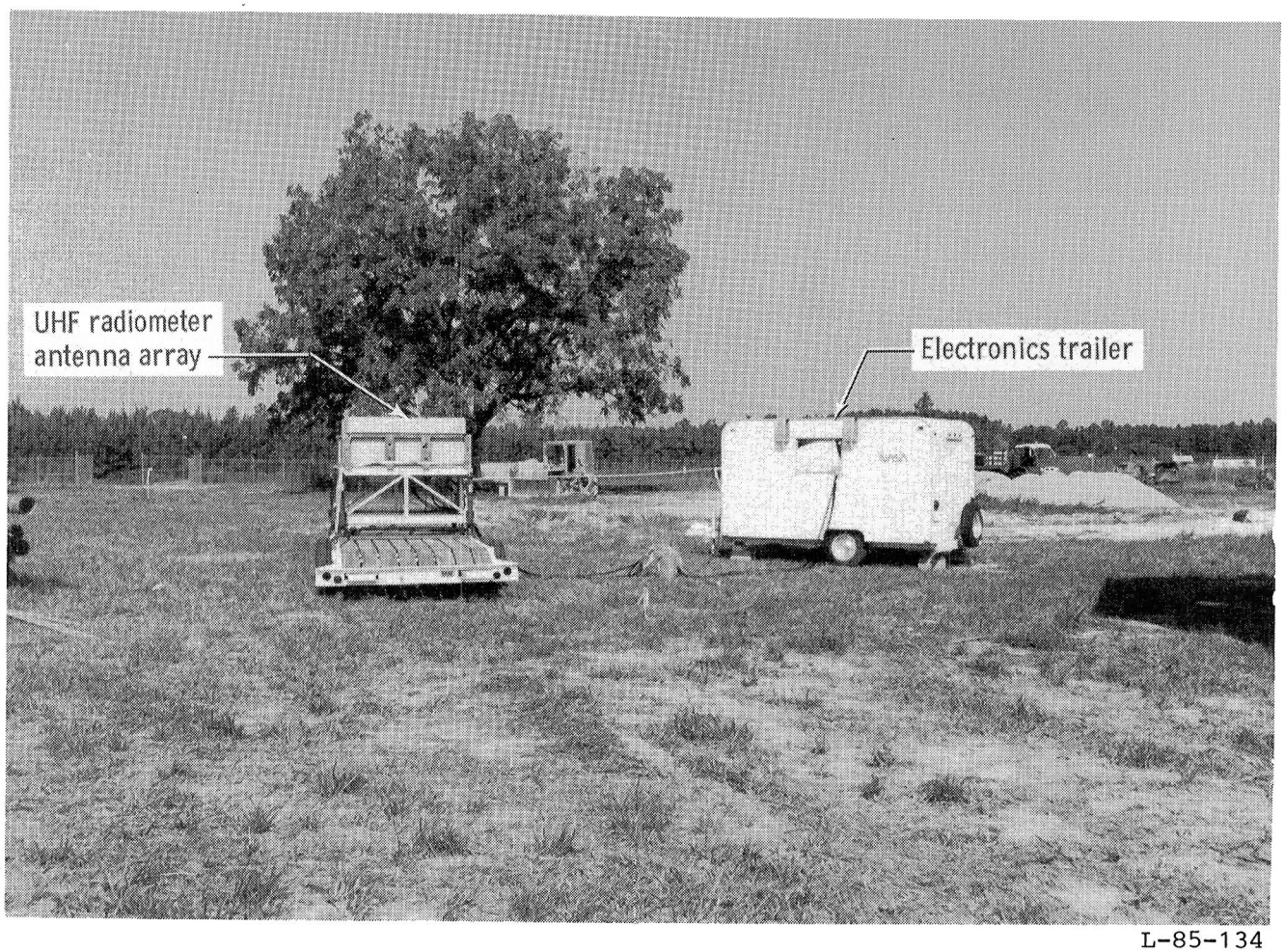

L-85-134

Figure 21.- UHF radiometer antenna and electronics trailer in remote field installation for RFI testing and sky temperature measurements.

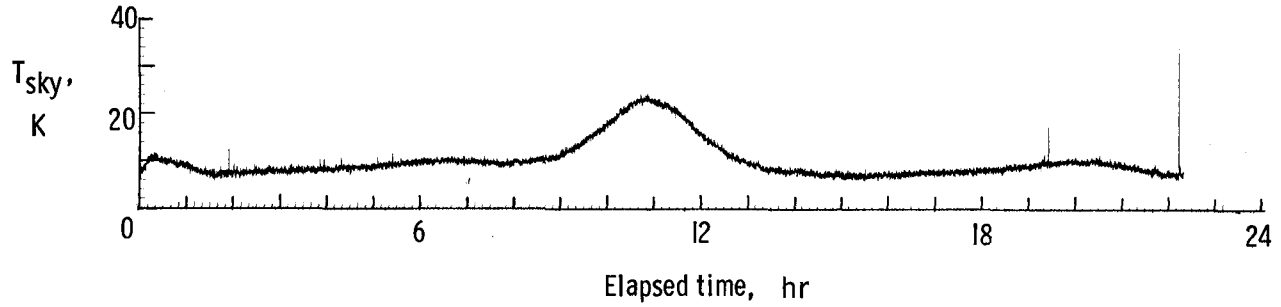

Figure 22.- Sky temperature measurements from UHF radiometer system at a frequency of 611 MHz during a 24-hr period.

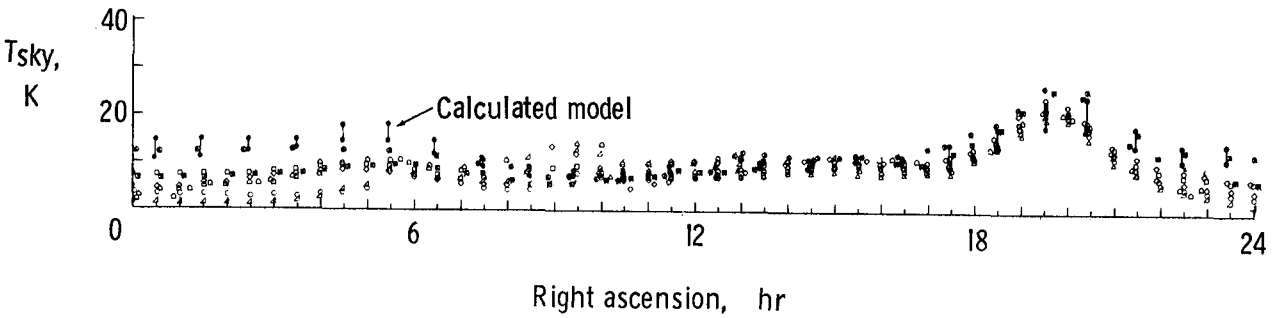

Figure 23.- Comparison of UHF radiometer zenith sky temperature measurements as a function of celestial right ascension with calculated model at 611 MHz over several 24-hr periods during August-September 1983 (37° 05' north declination).

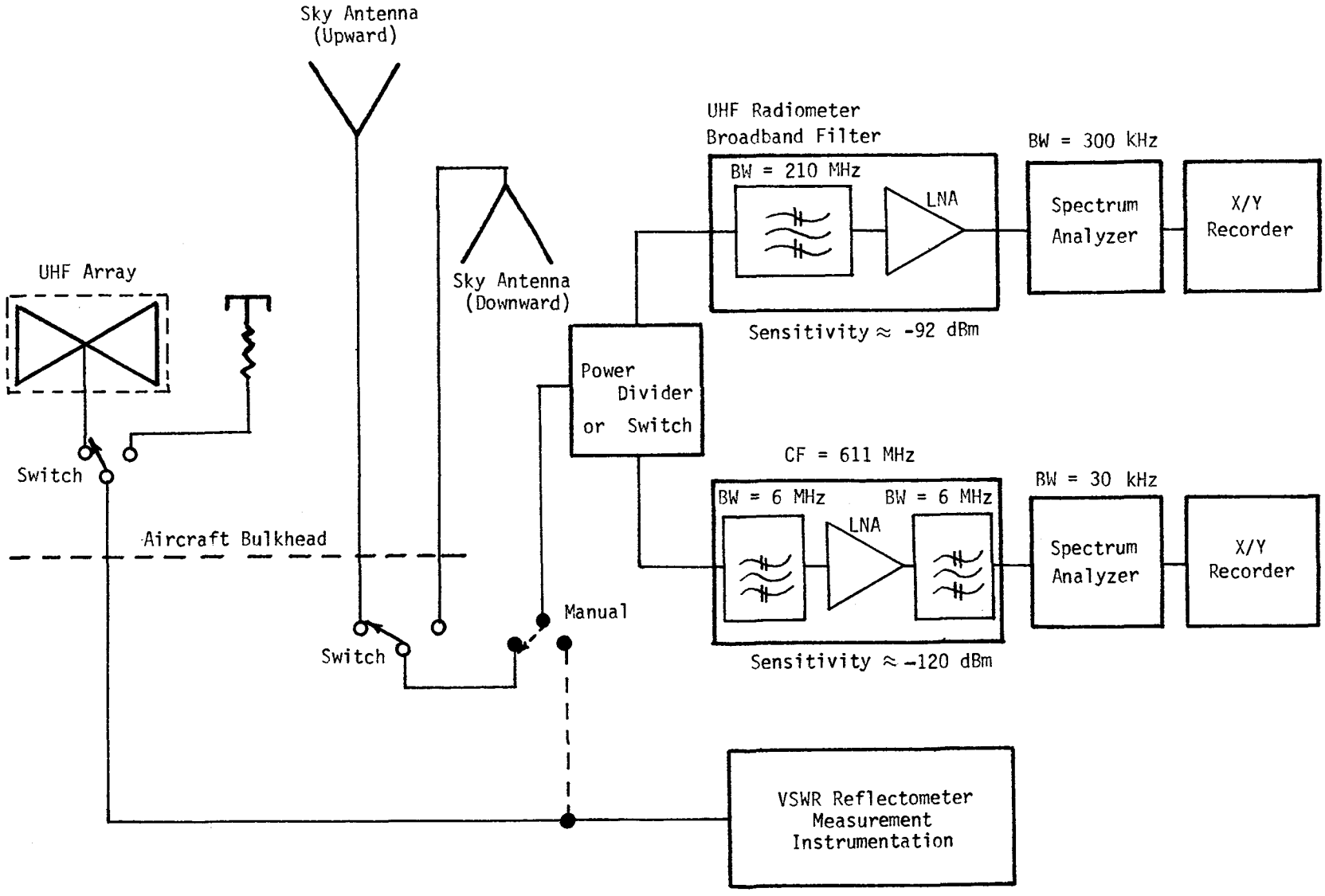

(a) Instrumentation for RFI measurements.

Figure 24.- Instrumentation for UHF radiometer flight measurement tests.

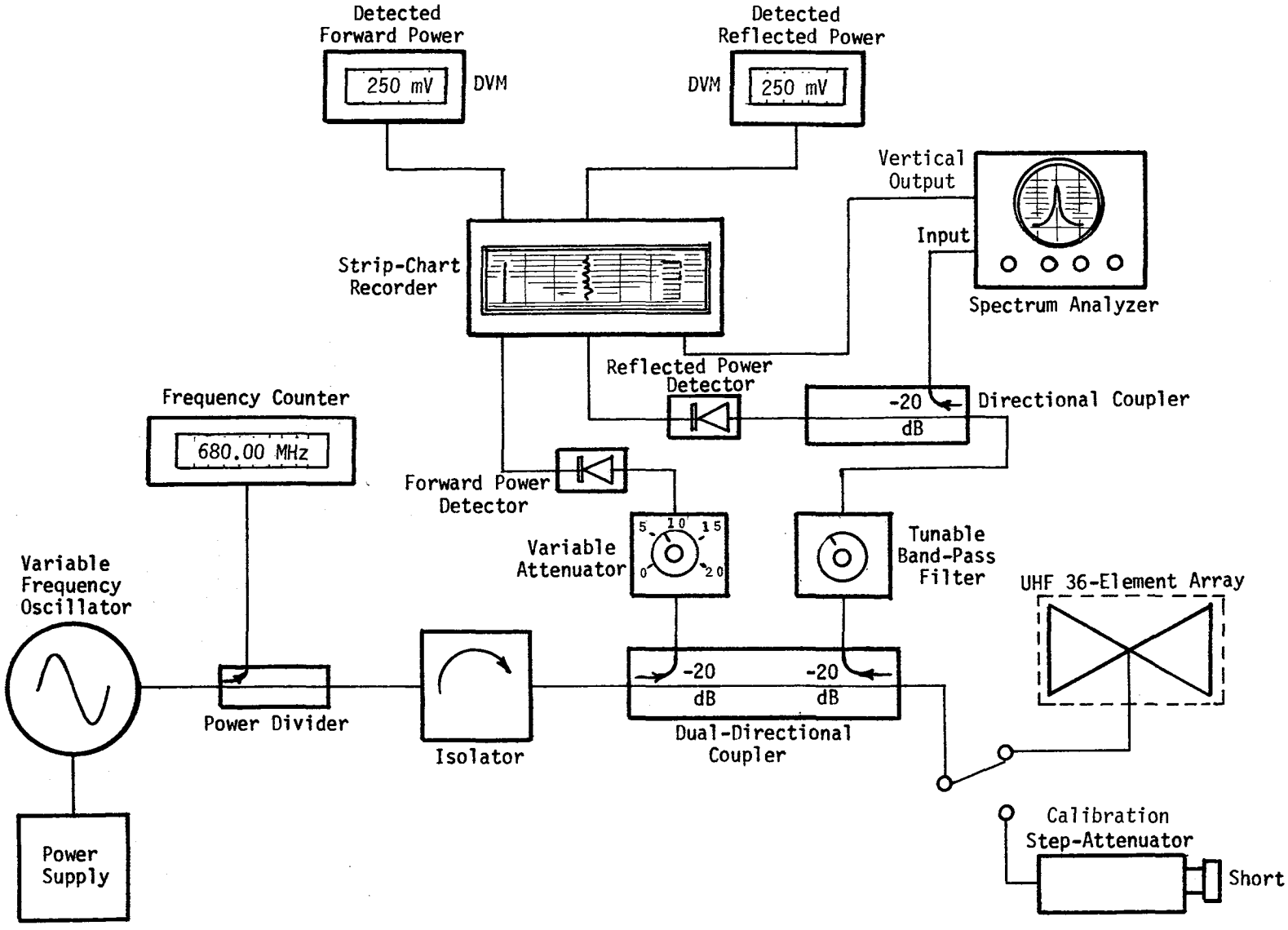

(b) Instrumentation for VSWR reflectometer measurements.

Figure 24.- Concluded.

L-82-8881

Figure 25.- Instrumentation for UHF radiometer antenna flight test measurements.

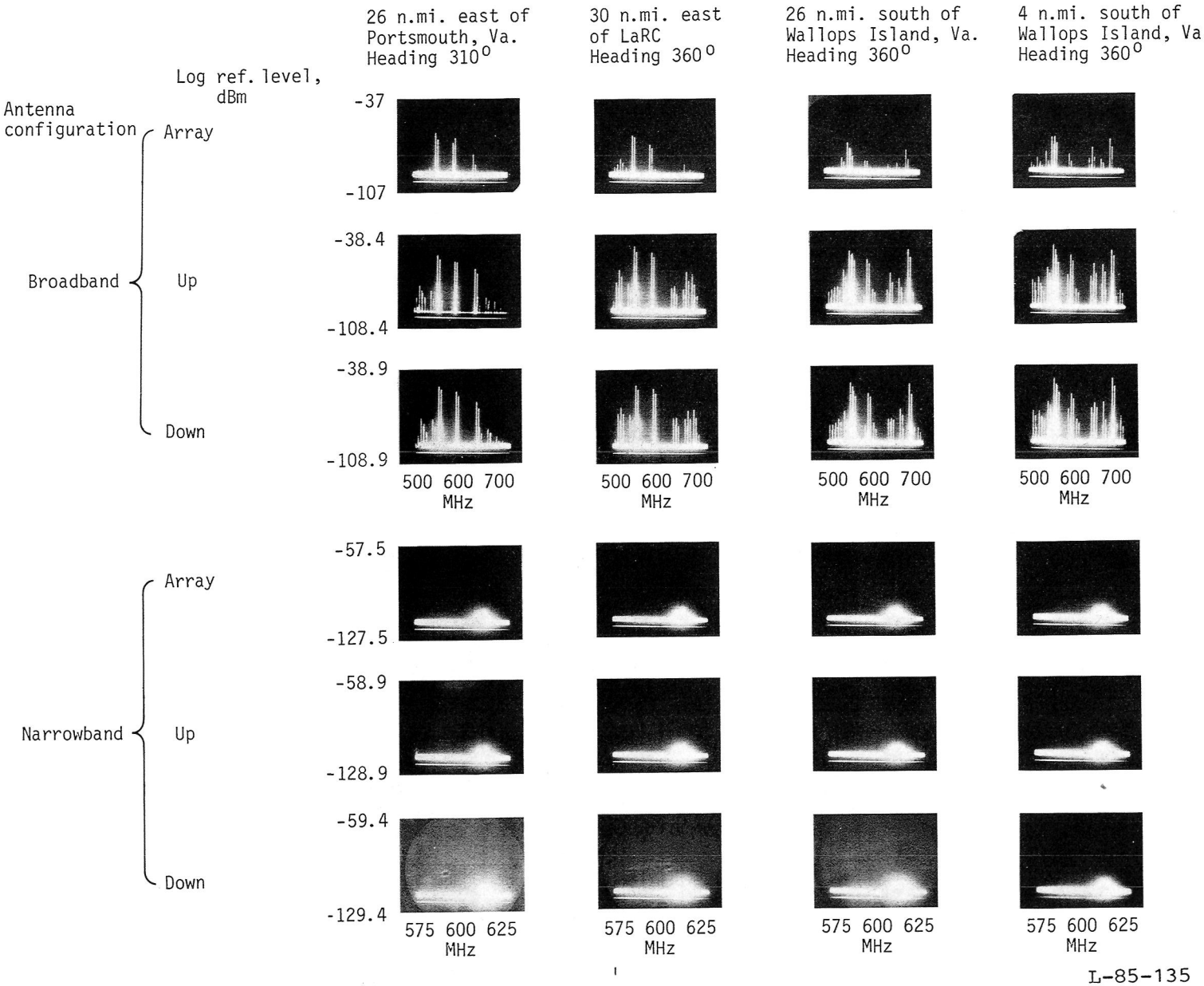

(a) Aircraft altitude of 1000 ft (304.8 m); east of Virginia coast.

Figure 26.- Composite photograph of broadband and narrowband RF spectrum displays (signal level as a function of frequency) for three antenna configurations. Measurements made from NASA P-3 aircraft.

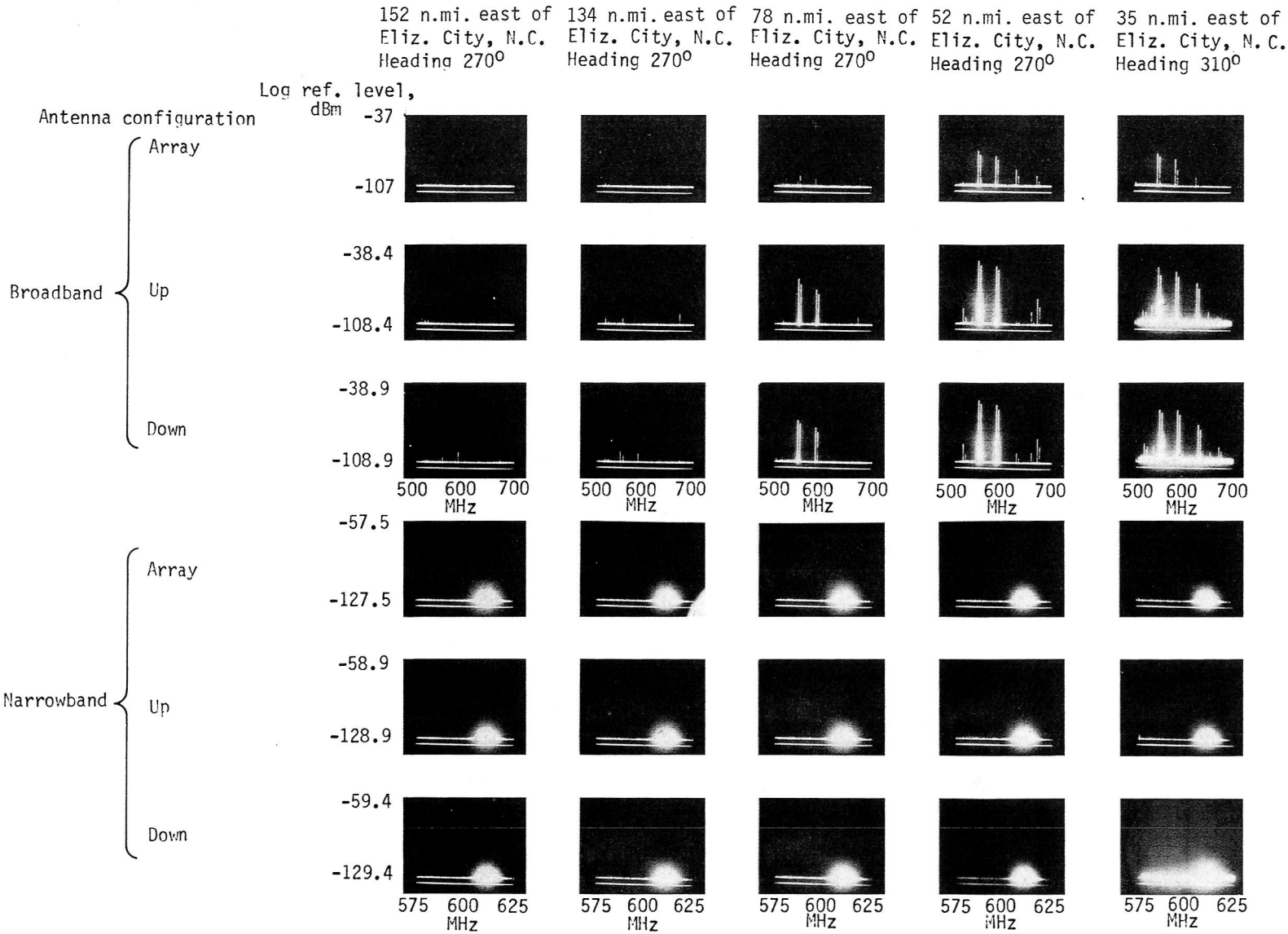

(b) Aircraft altitude of 1000 ft (304.8 m); east of Elizabeth City, North Carolina.

Figure 26.- Continued.

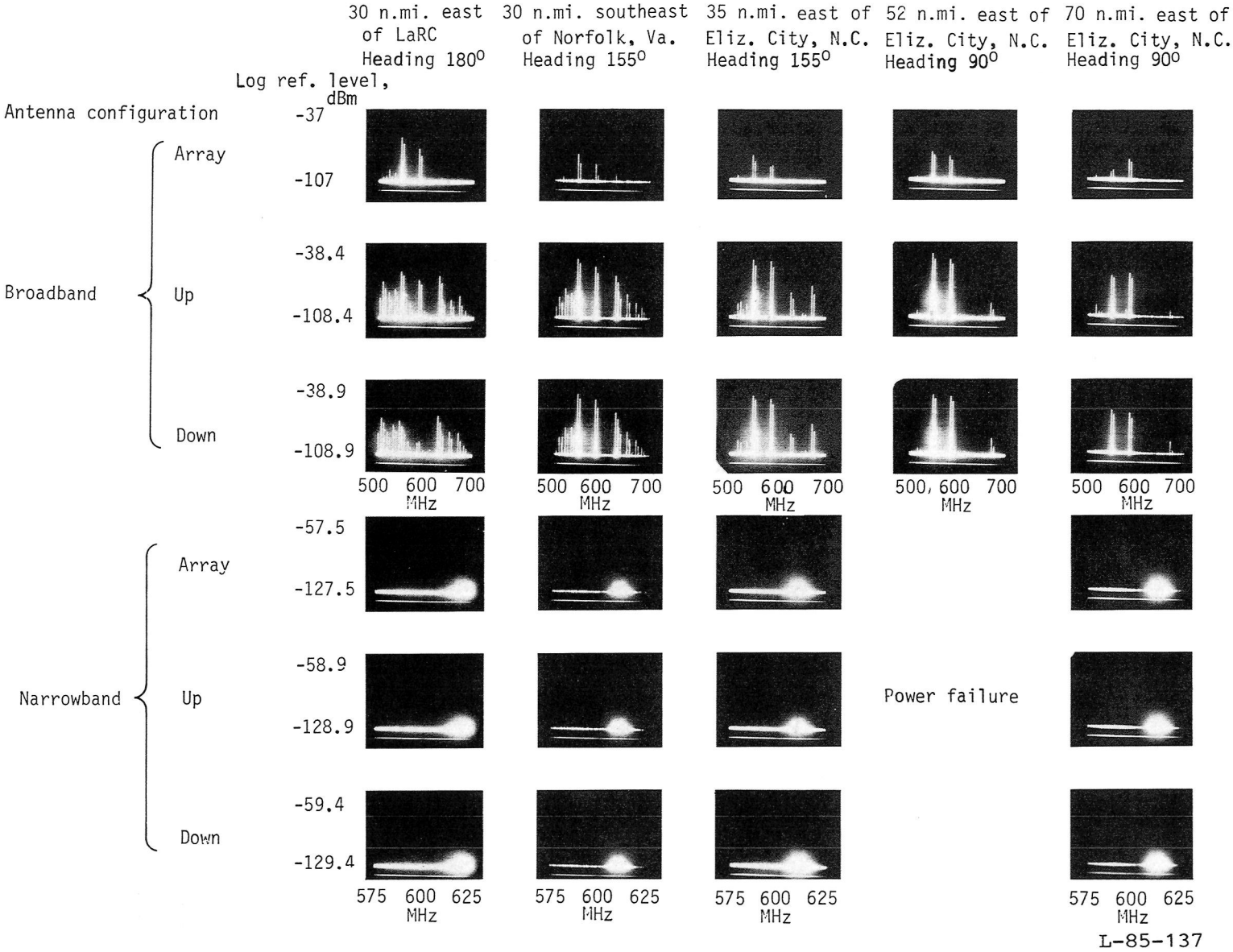

(c) Aircraft altitude of 500 ft (152 m); east of Virginia/North Carolina coast.

Figure 26.- Concluded.

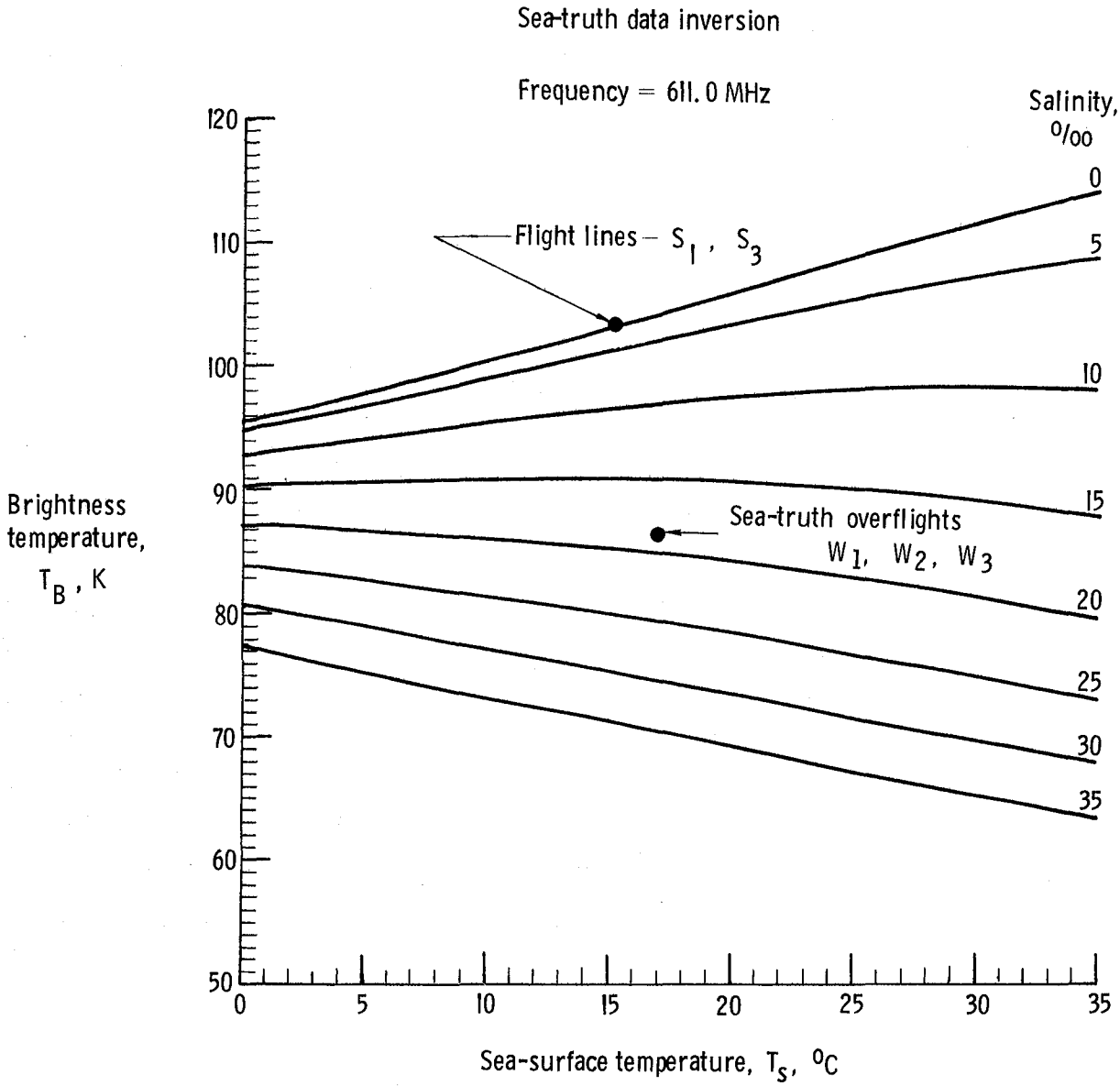

Figure 27.- Brightness temperature as a function of sea-surface temperature for several sea-salinity values, with measurement values determined during two flight lines as indicated.

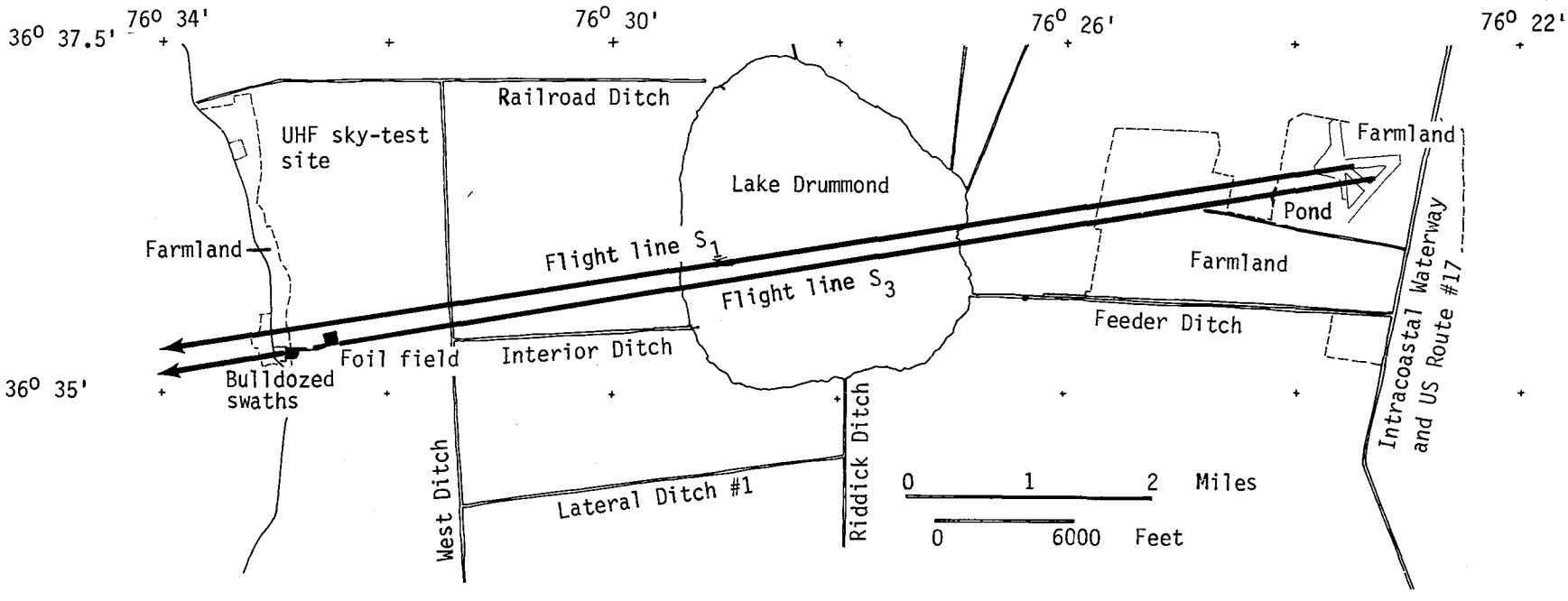

Base maps = Corapeake and Lake Drummond (N.C. and Va.)
U.S. Geological Survey 7½-minute quadrangles

Figure 28.- Map of Great Dismal Swamp, Virginia, showing flight line directions and location of foil field.

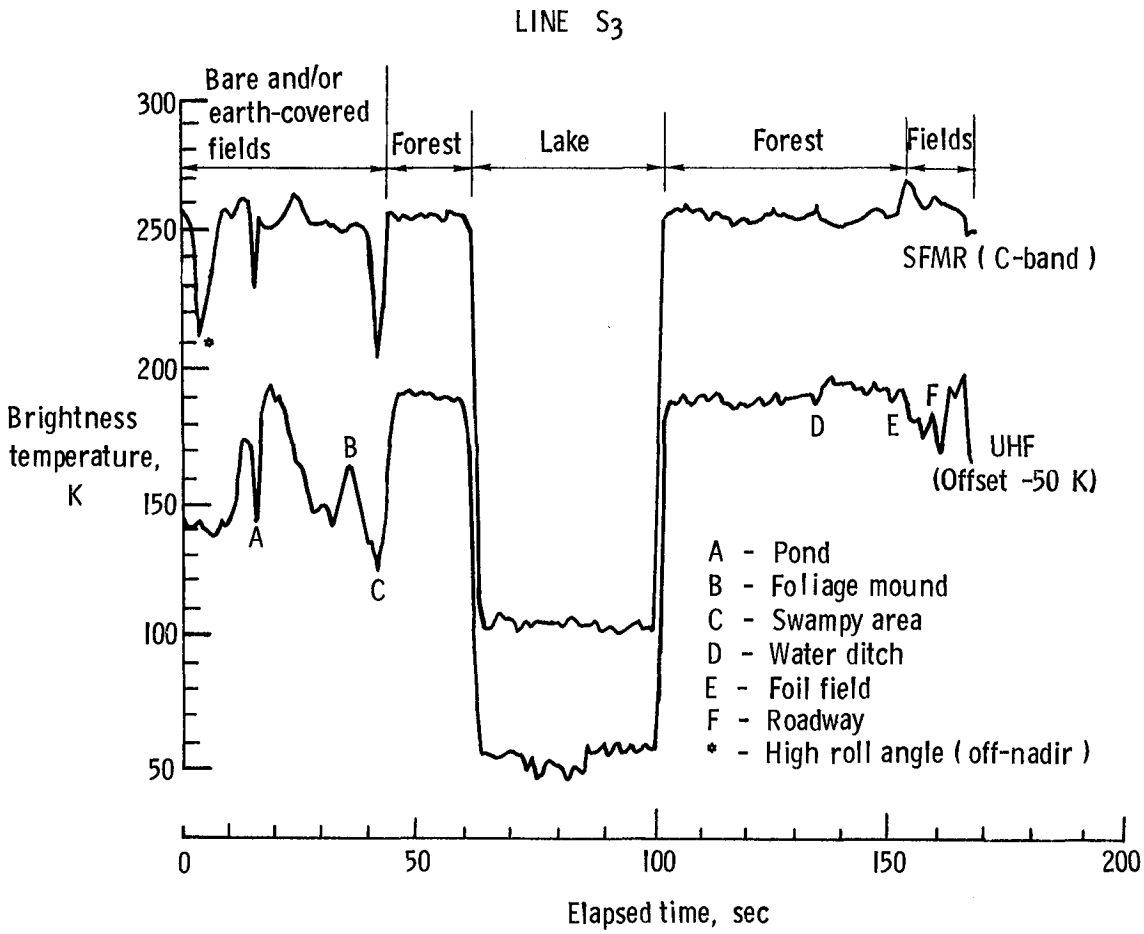

Figure 29.- Comparison of brightness temperature measurements made by C-band and UHF radiometers for various geographical conditions.

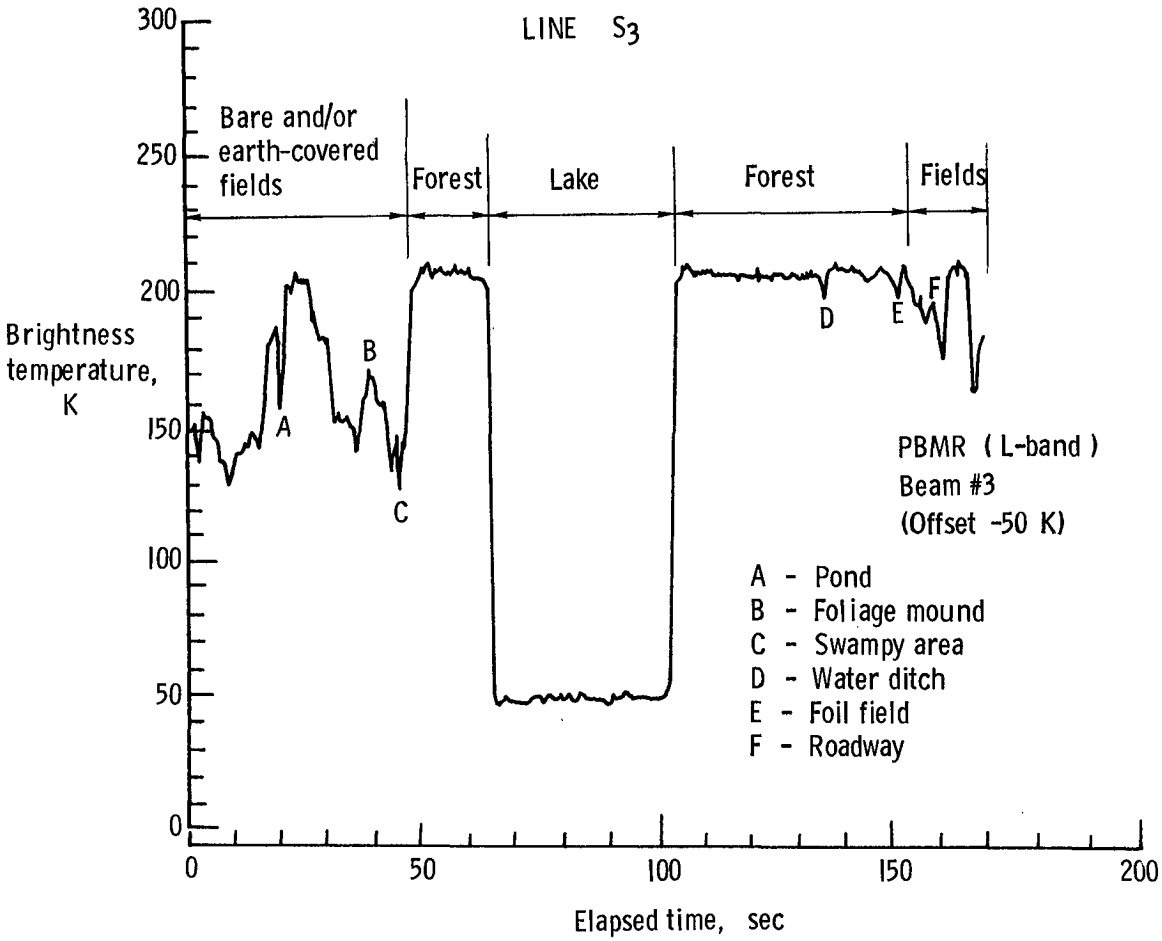

Figure 30.- Brightness temperature measurements made by L-band radiometer for various geographical conditions.

Standard Bibliographic Page

1. Report No.	2. Government Accession No.	3. Recipient's Catalog No.
NASA TP-2504		

4. Title and Subtitle	5. Report Date
Development of a UHF Radiometer	December 1985
	6. Performing Organization Code: 506-58-23-04
7. Author(s): Bruce M. Kendall, Hans-Juergen C. Blume, and Aubrey E. Cross	8. Performing Organization Report No.: L-16006
9. Performing Organization Name and Address: NASA Langley Research Center, Hampton, VA 23665-5225	10. Work Unit No.
	11. Contract or Grant No.
12. Sponsoring Agency Name and Address: National Aeronautics and Space Administration, Washington, DC 20546-0001	13. Type of Report and Period Covered: Technical Paper
	14. Sponsoring Agency Code

15. Supplementary Notes

16. Abstract

A wideband multifrequency UHF radiometer was initially developed to operate in the 500- to 710-MHz frequency range for the remote measurement of ocean water salinity. However, radio-frequency interference required a reconfiguration to operate in the single-frequency radio astronomy band of 608 to 614 MHz. Details of the radiometer development and testing are described. Flight testing over variable terrain provided a performance comparison of the UHF radiometer with an L-band radiometer for remote sensing of geophysical parameters. Although theoretically more sensitive, the UHF radiometer was found to be less desirable in practice than the L-band radiometer.

17. Key Words (Suggested by Authors(s))	18. Distribution Statement
Radiometer Remote sensing Oceanography Soil moisture UHF	Unclassified - Unlimited Subject Category 33

19. Security Classif.(of this report)	20. Security Classif.(of this page)	21. No. of Pages	22. Price
Unclassified	Unclassified	56	A04

For sale by the National Technical Information Service, Springfield, Virginia 22161

NASA-Langley, 1985

National Aeronautics and
Space Administration
Code NIT-4

Washington, D.C.
20546-0001